UNIVERSITY OF CALIFORNIA SAN DIEGO

Development of Structural Amorphous Metallic Fibers

A Thesis submitted in partial satisfaction of the requirements
for the degree Master of Science

in

Materials Science and Engineering

by

Travis Lawrence

Committee in charge:

Professor Olivia Graeve, Chair
Professor Javier Garay
Professor Vitali Nesterenko

2022

The Thesis of Travis Lawrence is approved, and it is acceptable in quality and form for publication on microfilm and electronically.

University of California San Diego

2022

DEDICATION

I dedicate this work to my parents for allowing me to pursue my undergraduate degree at Texas A&M University, where I was able to start my career as a Naval Officer and become who I am today. You guys were able to open the door for me to write my own ticket and I can't thank you enough for that.

To the United States Navy, who has given me the opportunity to attend this university under the Fleet Scholars Education Program. I am truly appreciative for the opportunity to pursue my master's degree while on shore tour and humbled to be one of the candidates chosen for this competitive program.

Lastly, to my wife Andrea. Thank you for accompanying me on late nights in the office while I meticulously created "dot patterns" or was re-watching a quarter of lectures the night before an exam. You picked up the slack and were always encouraging when I needed it. Your hard work and dedication in your own career continue to be an inspiration to me. I truly appreciate the sacrifices you have made along the way to allow me to excel in this program.

TABLE OF CONTENTS

LIST OF ABBREVIATIONS

SAM: Structural Amorphous Metal

I.D.: Inner Diameter

O.D.: Outer Diameter

PVC: Polyvinyl Chloride

PEI: Polyetherimide

HDR: High Dynamic Range

SPS: Spark Plasma Sintering

BMG: Bulk Metallic Glass

SEM: Scanning Electron Microscopy

T_g: Glass Transition Temperature

GFA: Glass Forming Ability

R_c: Cooling Rate

SCLR: Super Cooled Liquid Region

LIST OF FIGURES

LIST OF TABLES

ACKNOWLEDGEMENTS

Thank you to Dr. Olivia Graeve for allowing me to join your lab group and work on this exciting project. I appreciated your advice when I reached a fork in the road during my research and allowed me to create my own path.

A special thank you to Professor Garay and Professor Nesterenko for taking the time out of their busy schedules to be a part of my committee. I truly enjoyed your classes and the knowledge that I obtained, which has added great value to my research and professional development.

Thank you to Jake Bilyk for being someone that I could come to for help and bounce ideas off of during the design phase of this project. You were one of the few people that I could easily meet up with for help, especially during virtual learning.

Lastly, thank you to Nick at NJPB Glass for providing me with a plethora of advice along the way. Your many years of experience and willingness to share allowed me to bypass unnecessary learning curves and maintain my timeline. You were always willing to take a moment out of your busy schedule and answer any questions that I had.

ABSTRACT OF THE THESIS

Development of Structural Amorphous Metallic Fibers

by

Travis Lawrence

Master of Science in Materials Science and Engineering

University of California San Diego, 2022

Professor Olivia Graeve, Chair

SAM 2x5 is an iron based amorphous metal ($Fe_{49.7}Cr_{17.7}Mn_{1.9}Mo_{7.4}W_{1.6}B_{15.2}C_{3.8}Si_{2.4}$) that demonstrated the highest elastic limit during shock impact ever reported for a bulk metallic glass. In this research, SAM 2x5 powder was attempted to be thermally drawn into an amorphous metallic fiber via a draw tower assembled by the project team. Fibers were attempted to be drawn at varying temperatures ranging from 700 to 900˚C and varying

process speeds. Resulting fibers were analyzed under optical imaging and scanning electron microscopy, which showed that the SAM 2x5 powder was unable to create a continuous fiber via the thermal draw tower. The resulting fibers contained various amounts of small spherical SAM 2x5 particles entrapped inside the glass cladding, caused by the breakup of the solidified SAM 2x5 powder column.

CHAPTER 1- BACKGROUND

1.1- History

Metallic glasses are amorphous alloys that contain atoms of vastly different sizes, which creates low free volume in the structure. This causes the viscosity of the amorphous metals to be orders of magnitude higher than non-amorphous metals and alloys. The high viscosity prevents the atoms from rearranging to form an ordered lattice upon cooling (Figure 1.1), eliminating grain boundaries which are considered the weakest sections of crystalline materials. The lack of mobility of the atoms causes the lattice to be frozen in an amorphous (glassy) state that experiences low shrinkage during cooling and high resistance to plastic deformation. [1-2]

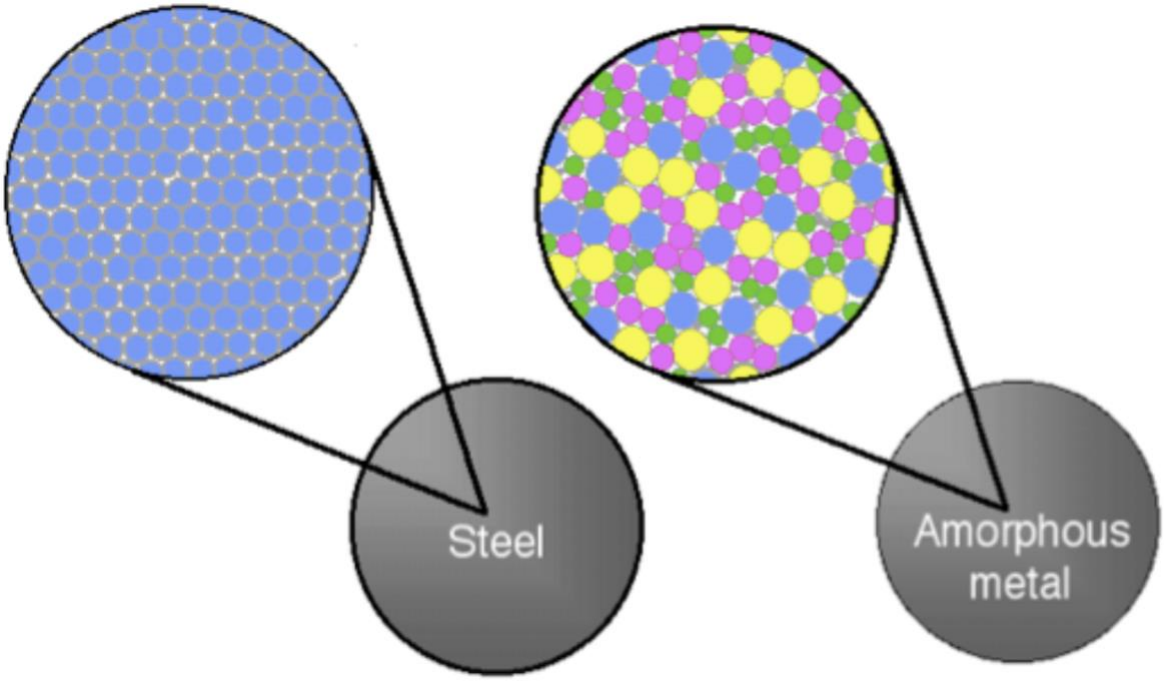

Figure 1.1- Visual Comparison of an Amorphous Metal Versus a Crystalline Metal [3]

Apart from thin films deposited at very low temperatures, metallic glasses were first developed in 1960 by Duwez at Caltech by forming an amorphous state of $Au_{75}Si_{25}$ via rapid

quenching at very high rates of 10^5-10^6 K/sec from 1300˚C to ambient temperature.[4] This high cooling rate was necessary to kinetically bypass the growth of crystalline phases and yield a frozen liquid atomic configuration, which are now called metallic glasses. This technique was utilized for decades to produce various binary metallic glasses; however, the necessity of a high rate of cooling limited the geometrical applications due to only being able to generate thin sheets.[2,5] Over the decades that followed, the techniques of vapor quenching and melt quenching have been thoroughly developed for producing a variety of multielement amorphous alloy phases. Plasma sputtering, chemical vapor deposition, and electron beam evaporation are some techniques that utilize producing amorphous alloy films from the vapor phase. Melt spinning, liquid atomization, and splat cooling are other popular techniques that utilize the liquid quench approach.[5,6]

Generally, glasses are formed through a vitrification process, which is cooled rapidly from its liquid state. If the cooling rate is slow enough the system kinetics allow the crystalline phase to form below the melting temperature, and the liquid is transformed into a crystalline solid structure. However, if the quench rate is fast enough the crystal phases will not have time to form and will be impeded. This results in a supercooled state, which is a metastable state compared to the crystalline state. After continued supercooling of the liquid, the viscosity of the liquid increases until the supercooled liquid reaches about 10^{13} Poise, which is 14-15 orders of magnitude higher than the viscosity at the melting temperature. This change in viscosity is called the glass transition temperature (T_g), in which the atomic structure is practically stationary and has formed a rigid glass. A materials glass forming ability (GFA) is a measure of the slowest cooling rate (R_c) a material can achieve while avoiding crystallization. With this, an alloy with a lower R_c has a better GFA than an alloy with a higher R_c.[7-9] A high GFA is a desirable property

in an amorphous metal because it would enable the production of bulk amorphous alloys by conventional casting processes with low cooling rates. This allows the applications of high GFA amorphous alloys to be significantly extended because of the easing of shape and dimension, which is arguably a limiting factor for amorphous metals.[9]

1.2- Mechanical Properties

Both glassy and crystalline metallic alloys have mainly metallic atomic bonds. However, despite this similarity between the two, bulk metallic glasses present properties significantly different compared to standard crystalline alloys. Bulk metallic glasses do not have the traditional slip systems that are found in crystalline metals. With the absence of dislocation-mediated slip, the resulting yield stress is much closer to the theoretical limit ($\sigma_y = E/20$) than their crystalline counterpart [7,10], shown in Figure 1.2. Figure 1.2 visually compares select bulk metallic glasses to over 1500 engineering alloys and related materials, showing that bulk metallic glasses have an unusual combination of high yield stress (σ_y) and low Young's modulus (E). Figure 1.2 also displays contours of elastic strain limit and resilience, for which metallic glasses have far exceeded any of the conventional materials. Lastly, the elastic strain limit in shear is very high and fairly uniform at 2.67%.[11] This elastic strain is a result of multiple shear bands occurring in a shear transformation zone, allowing the material to bend significantly without fracture, showing in Figure 1.3(d). The high elastic strain allows for applications in elastic hinges, pressure gages and flow meters, while the high resilience leads to applications requiring impact or energy absorption.[7,10]

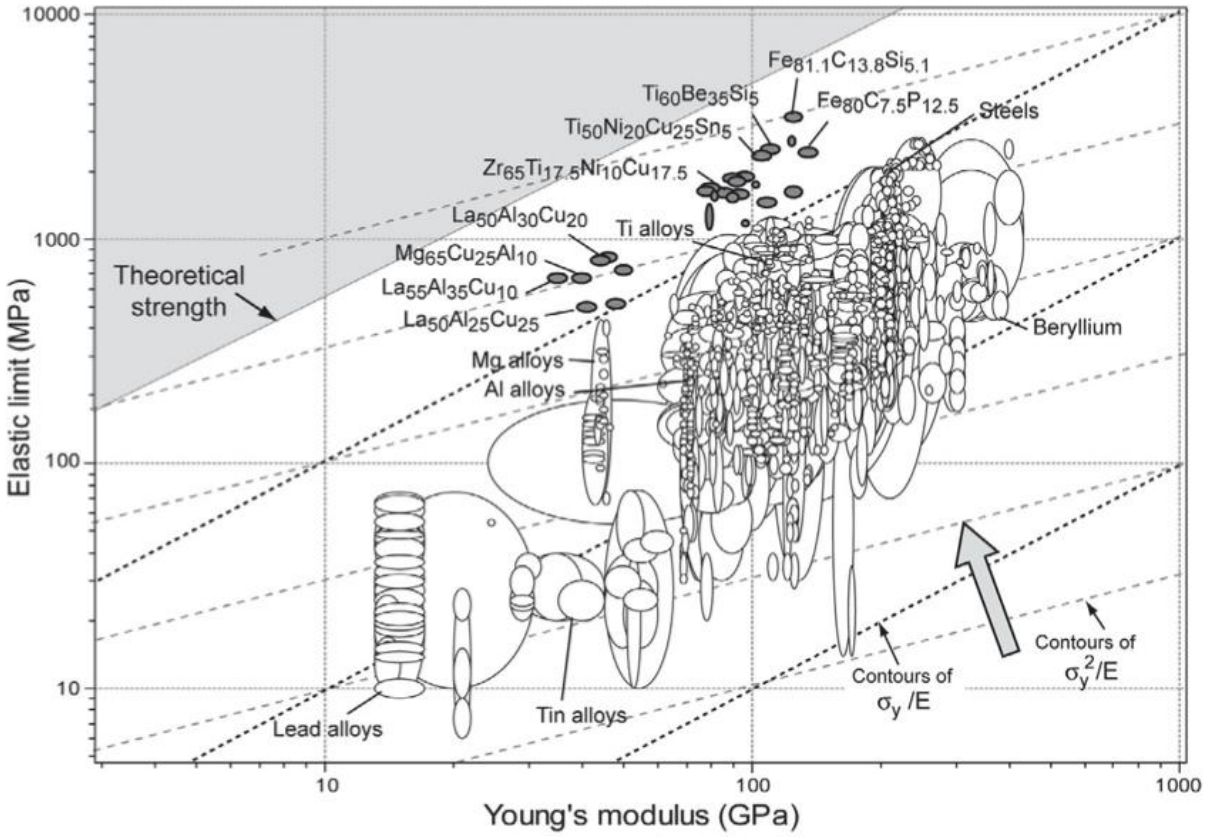

Figure 1.2- Elastic Limit (σ_y) Versus Young's Modulus (E) For 1507 Metals, Alloys, Metal-matrix Composites, and Metallic Glasses. The Contours Represent Elastic Strain Limit (σ_y/E) and Resilience (σ_y^2/E) [12]

As discussed, the lack of dislocations and slip systems in metallic glasses allow for exceptional yield strength and elastic properties. However, these attributes also result in undesirable effects on their plastic deformation after yield strain. At temperatures much below their T_g while under uni-axial tension or compression, metallic glasses shear fracture immediately after yielding without showing any appreciable macroscopic plastic strain, similar to inherently brittle material like typical silicate glasses.[13,14] However, their mode of failure is slightly different than that of a standard brittle material. The fracture surface occurs along the plane with the maximum resolved shear stress (~45˚) whereas typical brittle materials fracture at 90˚. Additionally, the fracture surface of the metallic glasses display features such as "vein patterns" or "river patterns".[7,15,16] The conflicting properties of brittle failure upon yield, but

ductile fracture surface features in metallic glasses have been attributed to severe localization of plastic deformation in microscopically narrow bands called shear bands.[13,14,17-23] Figure 1.3 (a), (b) display the results of one shear band causing brittle like failure during a tensile test. Figure 1.3 (c), (d) display the outcome of a bending test, where multiple shear bands are at play and the metallic glass is able to significantly plastically deform. This shows that bulk metallic glasses may be better suited for flexing/bending applications compared to tensile loading based on the effects of shear bands.

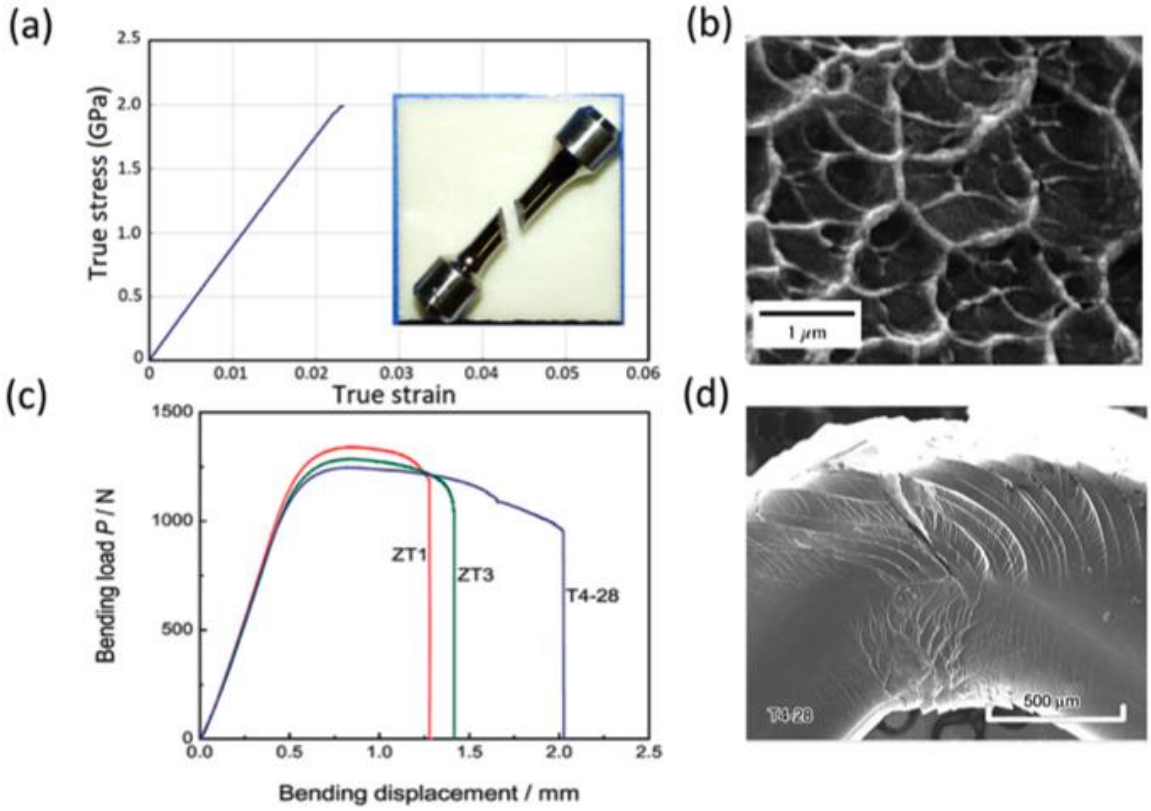

Figure 1.3- Ductility and Failure of Metallic Glasses Under Altered Loading Conditions at Room Temperature. (a) A Typical Tensile Fracture with Localized Plastic Deformation and No Ductility. (b) Vein Morphology Typical of "Ductile" Fractures. (c) Bending Load Test Showing Extensive Bending Ductility for Various Compositions. (d) Formation of Multiple Shear Bands Which Leads to the Extensive Bending Ductility [7]

1.3- SAM 2x5

SAM 2x5 ($Fe_{49.7}Cr_{17.7}Mn_{1.9}Mo_{7.4}W_{1.6}B_{15.2}C_{3.8}Si_{2.4}$) is an iron-based amorphous alloy known for its high corrosion resistance and is reported to be four to five times harder and more wear resistant than stainless steels and nickel-based alloys.[24,25] SAM 2x5-630 (a specific in situ composite of SAM 2x5 with slightly higher in situ crystalline precipitate) has the highest elastic limit during shock impact ever reported for a bulk metallic glass with a calculated value of 12.43 GPa.[26] SAM 2x5 powders are produced by gas atomization and milled using a high-energy ball mill.[27] The powder is then able to be solidified to ~95% of their theoretical density via spark plasma sintering (SPS). SPS utilizes the simultaneous application of pressure and electric current to heat the powder via Joule heating and densify the sample. The short processing times and lower processing temperatures needed for SPS are mainly responsible for arresting devitrification of the sample, yielding an amorphous solid bulk metallic glass.[27]

The glass transition temperature of SAM 2x5 is 579˚C.[25,28] As the sintering time and temperature are increased during densification, the crystallite size increases exponentially due to further departure above T_g, shown in Figure 1.4. Figure 1.4 compares SAM 2x5 with SAM 7 ($Fe_{48}Mo_{14}Cr_{15}Y_2C_{15}B_6$), a similar amorphous metal with approximately the same T_g but different crystallization characteristics when sintering temperature is increased. This becomes important when designing and selecting the experimental parameters used to create the draw tower, as well as altering the experimental variables based on findings discussed in the experiment section.

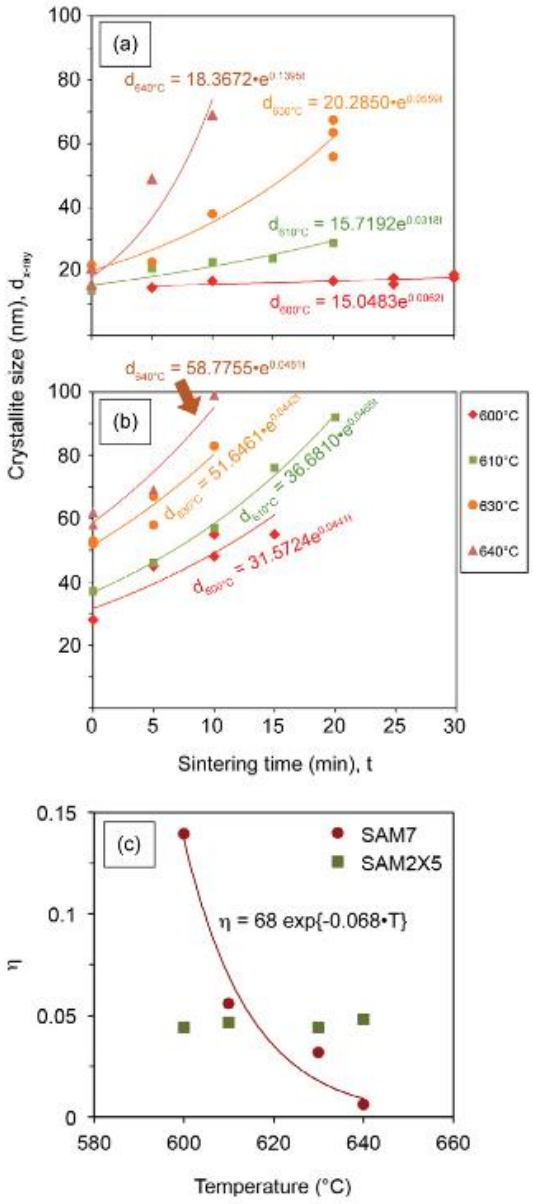

Figure 1.4- Change in Crystallite Size when Temperature and Sintering Time are Altered for (a) SAM 7 and (b) SAM 2x5, and (c) Change in Time-independent Exponential Variable with respect to Temperature [27]

1.4- Amorphous Metal Fibers

Processing of bulk metallic glasses require close attention to several variables. The largest hurdle to overcome is to avoid vitrification during processing and solidification for the bulk metallic glass to maintain its amorphous properties.[29] Cooling a material below its melting

temperature results in an increase in driving force for crystallization, which is quantified by the Gibbs free energy difference between the undercooled melt and the competing crystalline phases.[30-32] Because of this, bulk metallic glasses can generally be processed via two different approaches.

The first is direct casting, where an amorphous melt must be inserted into a mold and cooled sufficiently fast before the crystalline phases develop. Based on the relatively long time it takes to fill a mold cavity combined with fast cooling rates, only a limited range of thin geometries can be developed.[29] The second approach is to reheat a bulk metallic glass into the supercooled liquid region (SCLR) where the glass relaxes into a metastable liquid before it crystallizes. This process is called thermoplastic forming, which takes advantage of the softening of bulk metallic glasses upon heating above the glass transition temperature and the materials thermal stability, similar to that of thermoplastics. Thermal stability is a way to quantify the bulk metallic glass's ability to retain its amorphous structure when heated above its glass transition temperature,[29] providing a processing window that is fairly large for a variety of bulk metallic glasses.[33] Based on the large processing window, the already densified SAM 2x5 samples the project team has, and the lower processing temperatures required, reheating the SAM 2x5 samples into the SCLR to attempt to generate fibers was selected for this project.

Sorin et al.[34] was able to successfully generate micro- and nanoscale fibers via thermal drawing and was the basis for this project's design. It began by preparing a macroscopic preform made up of a platinum based metallic glass core ($Pt_{57.5}Cu_{14.7}Ni_{5.3}P_{22.5}$) and a supporting cladding (typically a thermoplastic polymer or glass, in this case they used polyetherimide (PEI)), shown in Figure 1.5. The cladding undergoes continuous plastic deformation during the draw process and supports most of the stresses induced during deformation. For the cladding and

the metallic glass to be co-drawn together, they must soften within the same temperature range, exhibit compatible viscosities at the processing temperature, resist crystallization, and the metallic glass should have slow crystallization kinetics at the drawing temperature.[35]

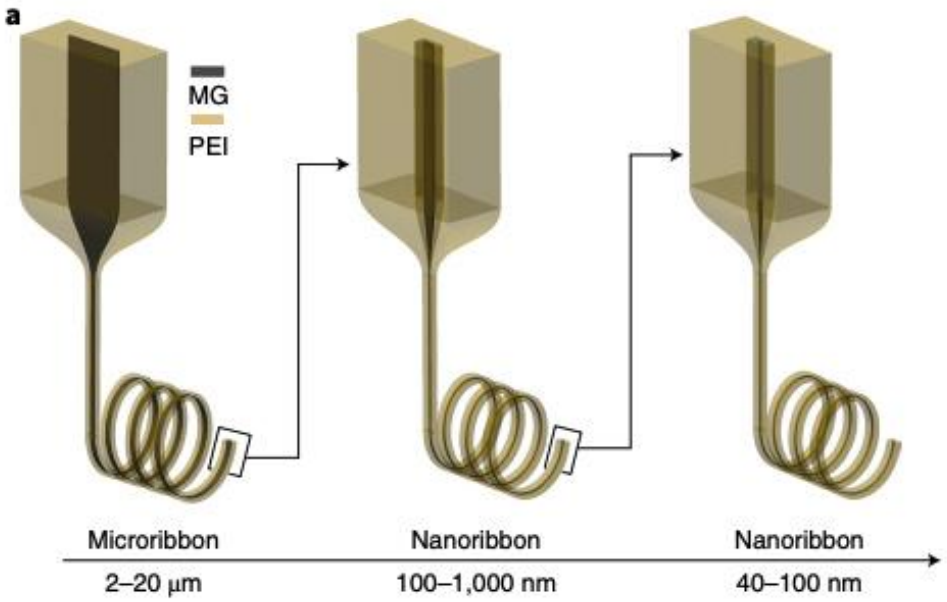

Figure 1.5- Visual of the Fiber Fabrication Process Showing a Metallic Glass Core in a Polyetherimide Cladding Reduced to a Nanoscale Ribbon via Multiple Draws [34]

In this fabrication, their goal was to develop metallic glass nanoscale ribbons to be used on optoelectronics and neuroscience. The generation of the macroscopic preform and the method of thermally drawing the preform in a thermal draw tower was deemed appropriate for the generation of SAM 2x5 fibers. With this, the SAM 2x5 would be encapsulated inside of a cladding with similar thermal properties to form a preform. The preform would then be thermally drawn at temperatures higher than $T_{g,\,SAM2x5}$ = 579˚C (residing in the SCLR of SAM 2x5) in a draw tower. The overarching process of a thermal draw tower is depicted below in Figure 1.6.

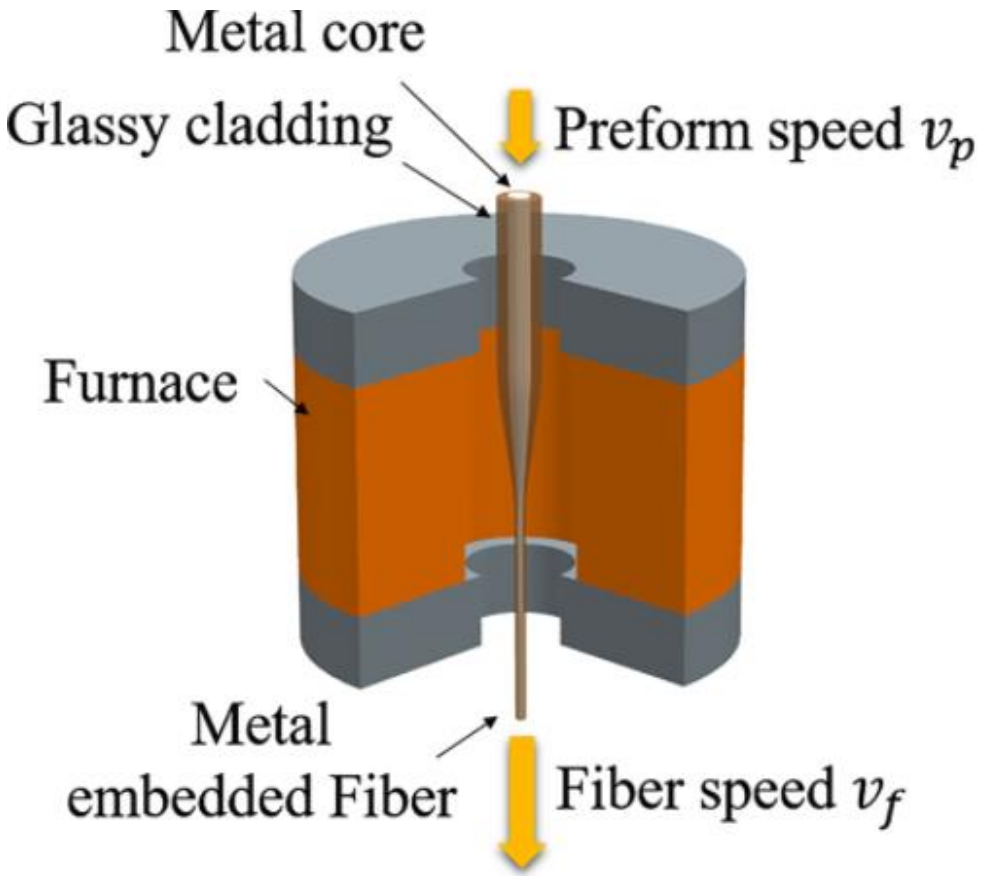

Figure 1.6- Visual Representation of Fiber Drawing [36]

Figure 1.6 displays what is happening inside of the furnace during fiber generation. As the preform is heated into the SCLR by the furnace, it becomes workable and deforms (necks down) into a fiber. The preform speed is controlled by a downfeed mechanism and the fiber speed is controlled by a capstan, discussed in the design section.

CHAPTER 2- DESIGN

2.1- Preform

The first step in beginning the design phase of this project was to determine a cladding material that would appropriately pair with SAM 2x5 in order to create the preform. The cladding material is present to assist with the mechanical stresses induced on the SAM 2x5 during the draw and to keep the SAM 2x5 discs consolidated in a stacked manner. As discussed, the cladding must have similar thermal properties as SAM 2x5 to be able to draw together. Soda lime glass and lead glass were chosen based on having a glass transition temperature of 525˚C[37] and 430˚C[38] and a softening temperature of 720˚C[37] and 630˚C[38] respectively, which corresponds well with the glass transition temperature of SAM 2x5 ($T_{g,\ SAM2x5}$ = 579˚C). Borosilicate glass was also used in the initial experiments to evaluate a preform with a much higher softening temperature ($T_{softening}$ = 821˚C)[39], in addition to verifying the initial operation of the draw tower.

The glass tubes were chosen as a convenient way to slide the preexisting SAM 2x5 discs into the tube in a stacking fashion. The SAM 2x5 discs were later changed to SAM 2x5 powder based on initial experiments and observations. The glass tubes have an I.D. of 7.58 mm and an O.D. of 10.23 mm to allow a sufficient core to cladding ratio of about 1.5. The top of the glass tubes have a flared edge to allow ease of access when inserting the SAM 2x5 discs into the tube and attaching the vacuum pump attachment to the top of the tube during the draw. The bottom of the tubes have a teardrop appendage to provide an access point to initiate the draw with manual force if necessary. The tubes were manufactured to a length of 60 cm to permit multiple experiments on a single glass tube.

2.2- Furnace

Once the size and length of the preform was established, a furnace was chosen to supply the heat necessary to initiate the draw. A tubular furnace was chosen to let the preform pass through the center of the furnace unobstructed, shown in Figure 2.1. This will allow the preform to lower into the top, neck down into a fiber, then exit the bottom of the furnace in a continuous manner. The furnace was designed to reach maximum temperature of 900°C, which was deemed adequate since the glass transition temperatures and softening temperatures of the materials making up the preform fall below this maximum. A lower temperature furnace allows design simplicity since the furnace could be operated in an open-air environment, compared to other higher temperature furnaces that require an inert controlled atmosphere. The furnace is equipped with a 6” single zone heated length, and a 1” unheated length on either end. It has a 1.5” I.D. stainless steel protection liner that is replaceable if the glass cladding was to be inadvertently stuck to the inner wall of the furnace during experiments. Lastly, a temperature controller provides a means to change the set furnace temperature, with a type “K” thermocouple to monitor the actual temperature inside.

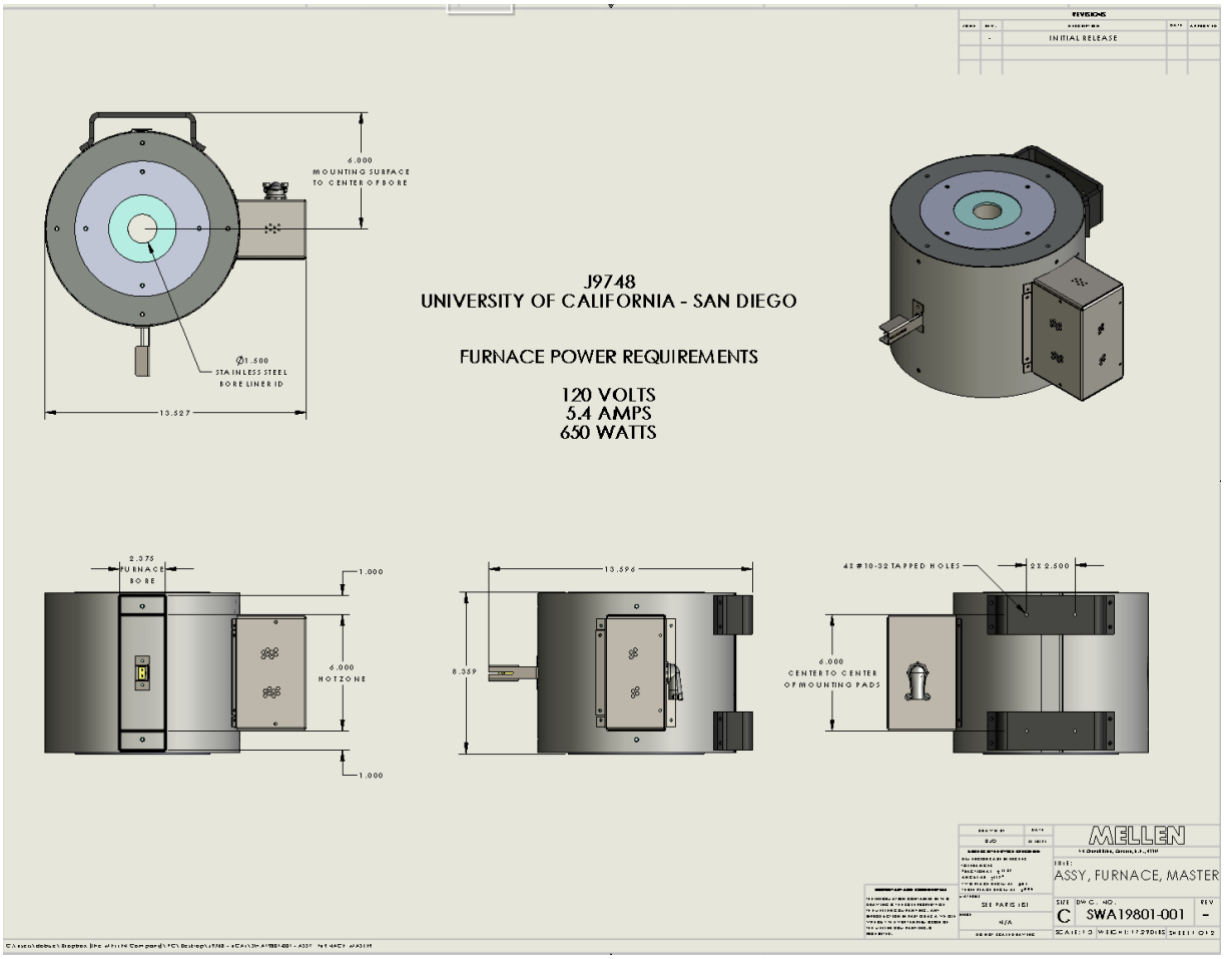

Figure 2.1- Engineering Drawing of the Tubular Furnace

2.3- Downfeed

A mechanism to supply the downfeed for the preform was the next component to consider. The downfeed must move the preform in a linear motion through the centerline of the furnace at a steady rate in order to establish a continuous process once the fiber draw is initiated. A linear slide from Zaber Technologies was chosen based on meeting these criteria. As shown in Table 2.1, the minimum speed and resolution are very precise, which gives the operator the ability to accurately adjust the speed of the downfeed. The downfeed moves via a worm gear attached to an electric motor, which slides the mounting platform up and down. The mounting platform only protrudes 35.8 mm from the mounting plate on the back of the structure, so an

attachment was designed and created (Figure 2.2) to allow the preform to be held at 152.4 mm away from the mounting plate, corresponding to the centerline of the furnace. The attachment was designed to be adjustable via a hex key, allowing for any minor changes to be made upon assembly. Lastly, an adjustable tube clamp is included to hold the preform during experiments and change preforms as necessary.

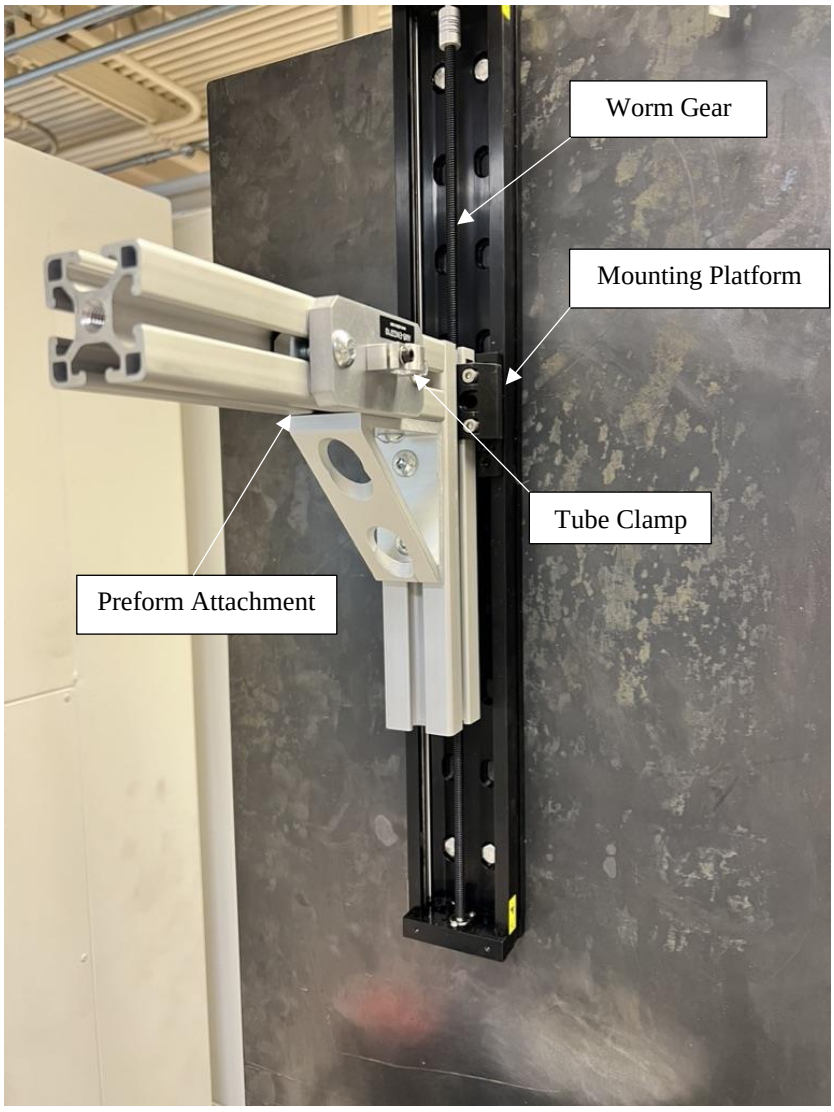

Figure 2.2- Adjustable Attachment for Linear Slide

Table 2.1- LSQ450A (Linear Slide) Data Sheet

Specification	Value	Alternate Unit
Microstep Size (Default Resolution)	0.09921875 µm	
Built-in Controller	Yes	
Travel Range	450 mm	17.716"
Accuracy (unidirectional)	135 µm	0.005315"
Repeatability	< 2 µm	< 0.000079"
Backlash	< 15 µm	< 0.000591"
Maximum Speed	53 mm/s	2.087"/s
Minimum Speed	0.000061 mm/s	0.000002"/s
Speed Resolution	0.000061 mm/s	0.000002"/s
Encoder Resolution	500 CPR	2000 states/rev
Encoder Type	Rotary quadrature encoder	
Peak Thrust	275 N	61.7 lb
Back-driving Force	Non-back-driving	
Maximum Continuous Thrust	100 N	22.4 lb
Communication Interface	RS-232	
Communication Protocol	Zaber ASCII (Default), Zaber Binary	
Maximum Centered Load	500 N	112.1 lb
Maximum Cantilever Load	2000 N-cm	2832.2 oz-in
Guide Type	Recirculating Ball Linear Guide	
Vertical Runout	< 30 µm	< 0.001181"
Horizontal Runout	< 40 µm	< 0.001575"
Pitch	0.06°	1.047 mrad
Roll	0.03°	0.523 mrad
Yaw	0.03°	0.523 mrad
Stiffness in Pitch	150 N-m/°	116 µrad/N-m
Stiffness in Roll	225 N-m/°	78 µrad/N-m
Stiffness in Yaw	150 N-m/°	116 µrad/N-m
Maximum Current Draw	1450 mA	
Power Supply	24-48 VDC	
Power Plug	2-pin Screw Terminal	

Table 2.1- LSQ450A (Linear Slide) Data Sheet (Cont.)

Linear Motion Per Motor Rev	1.27 mm	0.050"
Motor Steps Per Rev	200	
Motor Type	Stepper (2 phase)	
Motor Rated Current	2300 mA/phase	
Inductance	2.2 mH/phase	
Default Resolution	1/64 of a step	
Data Cable Connection	Locking 4-pin M8	
Mechanical Drive System	Precision lead screw	
Limit or Home Sensing	Magnetic home sensor	
Manual Control	Indexed knob with push switch	
Axes of Motion	1	
LED Indicators	Yes	
Mounting Interface	M6 threaded holes and 8-32 threaded holes	
Operating Temperature Range	0 to 50 °C	
Vacuum Compatible	No	
RoHS Compliant	Yes	
Stage Parallelism	< 100 µm	< 0.003937"
CE Compliant	Yes	
Weight	2.30 kg	5.071 lb

2.4- Capstan

A fiber collection method was the last major component to determine. A cylindrical spool attached to a rotating motor was chosen to allow uniform tension to be applied to the preform while the fiber was being wrapped around the spool. The rotating assembly was also obtained from Zaber Technologies for ease of device communication, high rotational accuracy, and high continuous torque capabilities shown in Table 2.2. A PVC spool was designed and manufactured to attach to the rotating motor with a diameter of 167 mm. This diameter was selected to be able

to mount the spool as close to the furnace as possible, while still leaving a gradual enough curvature to not shatter the fibers as it is being wrapped around the spool. The linear slide and rotating spool motor communicate via a universal drive controller with a common link to a computer, in which the downfeed velocity of the linear slide and the rotational velocity of the capstan can be adjusted.

Table 2.2- RST120AK-T3A (Capstan) Data Sheet

Specification	Value	Alternate Unit
Built-in Controller	No	
Recommended Controller	X-MCC (48 V) Recommended	
AutoDetect	Yes	
Range	360°	
Backlash	< 0.05°	< 0.873 mrad
Encoder Type	None	
Motor Steps Per Rev	200	
Motor Type	Stepper (2 phase)	
Motor Connection	D-sub 15	
Default Resolution	1/64 of a step	
Mechanical Drive System	Precision Worm Gear	
Limit or Home Sensing	Magnetic home sensor	
Operating Temperature Range	0-50 °C	
Vacuum Compatible	No	
RoHS Compliant	Yes	
CE Compliant	Yes	

Part Number	Microstep Size (Default Resolution)	Accuracy (unidirectional)	Repeatability	Maximum Speed
RST120AK-T3A	0.00015625° (2.727 µrad)	0.16° (2.792000 mrad)	< 0.005° (< 0.087 mrad)	24°/s (4 rpm)

Table 2.2- RST120AK-T3A (Capstan) Data Sheet (Cont.)

Part Number	Maximum Centered Load	Maximum Cantilever Load	Guide Type	Stage Top Dimension
RST120AK-T3A	500 N (112.1 lb)	2000 N-cm (2832.2 oz-in)	Preloaded Ball Bearing	120 mm (4.724")
Part Number	**Angular Motion Per Motor Rev**	**Motor Rated Current**	**Motor Winding Resistance**	**Inductance**
RST120AK-T3A	2°	1500 mA/phase	2.4 ohms/phase	6.6 mH/phase
Part Number	**Minimum Speed**	**Speed Resolution**	**Maximum Torque**	**Maximum Continuous Torque**
RST120AK-T3A	0.000095°/s (1.658 µrad/s)	0.000095°/s (1.658 µrad/s)		1000 N-cm (1416.1 oz-in)
Part Number	**Maximum Angular Momentum**	**Motor Frame Size**	**Gear Ratio**	**Mounting Interface**
RST120AK-T3A	0.4 kg-m2/s	17	180:1	Kinematic with M2.5 and M6 threaded holes
Part Number		**Weight**		
RST120AK-T3A		2.40 kg (5.291 lb)		

2.5- Draw Ratio

To allow the neck down region to stay inside the furnace and have a consistent draw ratio, the speed of the downfeed versus the angular velocity of the spool are related by conservation of mass equation 1.[40]

$$\rho * v_{downfeed} * A_{preform} = \rho * v_{spool} * A_{fiber} \ , \ \rho = constant$$

$$v_{downfeed} * \frac{1}{4} \pi {D_{preform}}^2 = v_{spool} * \frac{1}{4} \pi {D_{fiber}}^2$$

$$v_{downfeed} * {D_{preform}}^2 = v_{spool} * {D_{fiber}}^2$$

$$D_{fiber} = D_{preform} * \sqrt{\frac{v_{downfeed}}{v_{spool}}} \quad (1)$$

The diameter of the fiber is related to the diameter of the preform by a reduction ratio, $\left(\frac{D_{preform}}{D_{fiber}}\right)^2$. Since the diameter of the preform is fixed at 10 mm, the diameter of the fiber will be about 1.4 mm based on a desired reduction ratio of 50. A reduction ratio of 50 was chosen based on thermal draw experiments performed on optical fibers in a similar manner.[41] With the reduction ratio selected, a downfeed velocity or angular spool velocity to be chosen. Once one of these parameters is arbitrarily chosen, then the other variable can be solved for. The linear velocity of the spool can be converted to angular velocity by equation 2.

$$v_{spool} = r_{spool} * \omega_{spool} \quad (2)$$

The angular velocity of the spool is necessary to be determined in radians/sec because the program used to control the rotating spool requires this input. In the experiment section, these parameters were adjusted based on findings from the fiber draw attempts.

2.6- SolidWorks Assembly

After all the individual components of the draw tower were determined, the parts were modeled into a SolidWorks assembly to ensure the relative sizes of the components were appropriate with respect to one another and a stand design could be developed. The individual parts were mated and constrained to the centerline of the furnace to ensure proper unobstructed travel of the preform. Once all parts were properly mated and constrained, a stand to hold all components in place was developed, shown in Figure 2.3. Figure 2.3 (a), (b) displays the various components of the draw tower constrained together. Figure 2.3 (c), (d) display the stand developed to hold the components in their appropriate places. The furnace between Figure 2.3 (a), (b) and Figure 2.3(c), (d) differs due to the furnace design being finalized between the rendering of the two assemblies, however the critical distance of 152.4 mm from the centerline

of the furnace to the mounting surface is unchanged between the two designs. Once the furnace design was finalized, the stand was created.

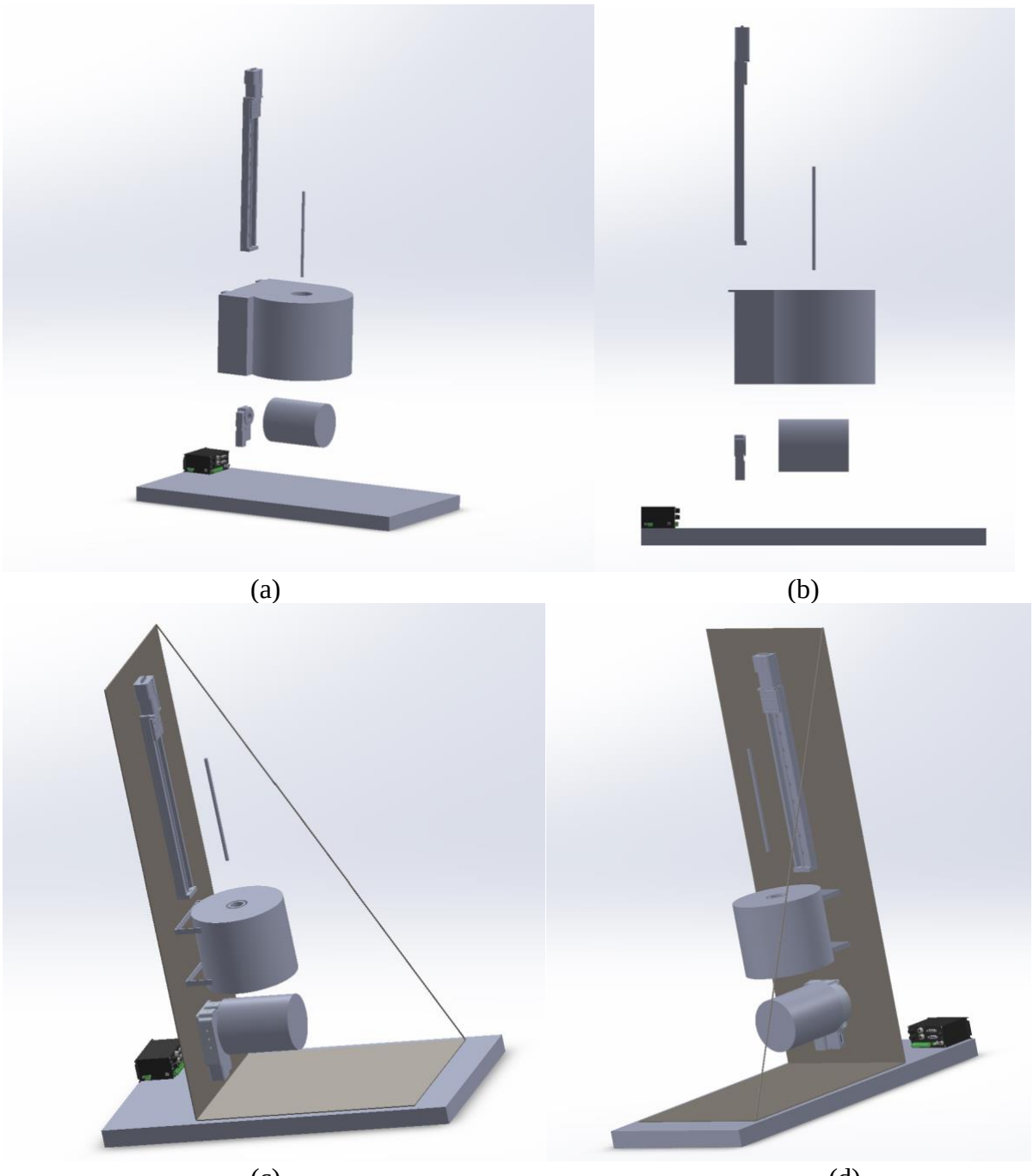

(a) (b)

(c) (d)

Figure 2.3- SolidWorks Assembly of Draw Tower

The stand was designed to be 50” tall and 18” wide, made of 1/8” steel. The bottom platform was designed to be 25” long to provide a large enough base support the vertical weight. A stabilizing bar was added to span diagonally across the stand to ensure the vertical component of the stand did not sway in any direction during operation and the added weight of the components did not cause the stand to bow inward. Lastly, a 2” lip was added to the back of the stand to ensure the stand did not fall backward and to further stabilize the assembly.

2.7- Physical Assembly

Once the assembly was finalized and all parts were received, the stand was laid flat and the components were physically laid out onto the stand to ensure proper spacing and alignment. The furnace was positioned such that the top of the first mounting bracket was 27” from the top of the stand to allow sufficient spacing for the linear slide attachment to not contact the furnace when at its lowest point. The furnace was mounted on the centerline of the stand by drilling a 5/32” hole into the steel corresponding to each of the 4 mounting holes of the furnace. The furnace was secured onto the stand using 4, 1/8” hex head stainless steel bolts, each with a corresponding washer and anti-slip nut.

The next component to be mounted was the linear slide. Since the linear slide required an attachment to securely hold the preform, the distance from the centerline of the attachment to the centerline of the linear slide had to be determined. This distance was measured to be 1.625” using calipers, resulting in the center of the linear slide to be positioned at 7.375” from the left edge of the stand. The linear slide was measured to be 2.5” wide, so to ensure the linear slide was in the correct position, the top and bottom left edges of the linear slide were positioned and marked to 6.125” from the left edge of the stand. The linear slide was then clamped in position to allow the stand to be uprighted. A plum bob test was performed to verify the linear slide

attachment was coincident with the center of the furnace. The plum bob test passed, and a borosilicate tube was inserted into the preform attachment to again ensure centerline with the furnace, shown in Figure 2.4. After all tests passed and measurements were verified, the linear slide was mounted to the stand by drilling a 5/16” hole into the steel corresponding to 4 mounting holes of the linear slide. The linear slide was secured to the stand using 4, 1/4” hex head stainless steel bolts, each with a corresponding washer and anti-slip nut.

Figure 2.4- Centerline Test of Linear Slide Prior to Mounting

Lastly, the capstan was mounted offset from the centerline of the furnace such that no lateral force would be applied to the fiber exiting the furnace. This was accomplished by

attaching the PVC spool to the rotating assembly and using the radius of the PVC spool (r=83.5mm, 3.28”) as an offset from the centerline of the furnace. The capstan was clamped to the stand and the assembly was again uprighted to perform another plumb bob test to ensure the plumb bob was tangential to the PVC spool. After this test passed and measurements were verified, the rotating assembly was mounted to the stand by drilling a 5/16” hole into the steel corresponding to 4 mounting holes of the rotating assembly. The rotating assembly was secured to the stand using 4, 1/4” circular hex key stainless steel bolts, each with a corresponding washer and anti-slip nut, resulting in the finalized assembly shown in Figure 2.5.

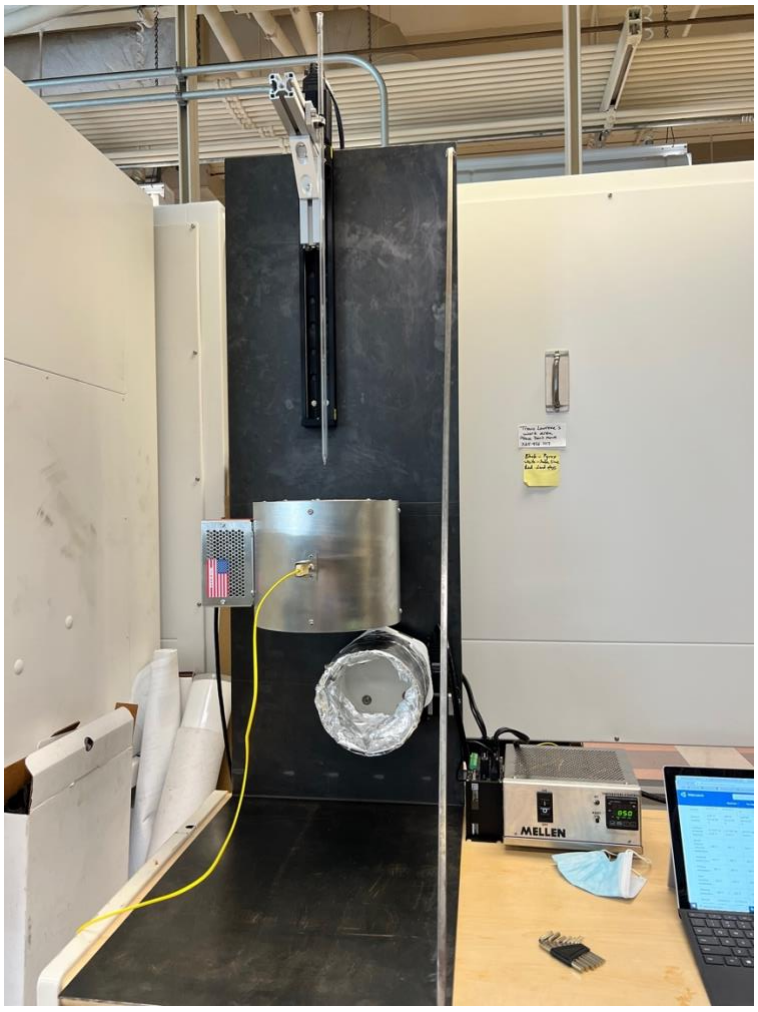

Figure 2.5- Finalized Draw Tower Assembly

2.8- Sample Preparation and Experimental Steps

Using the Zaber linear slide control software, the linear slide and preform attachment are raised to the starting (home) position on the linear slide. This allows a reference position to be established, as well as provide enough room between the preform attachment and the furnace to mount the preform in later steps. The preform attachment is moved in a linear direction by a worm gear that runs the length of the linear slide. The starting position of the linear slide attachment is shown in Figure 2.6.

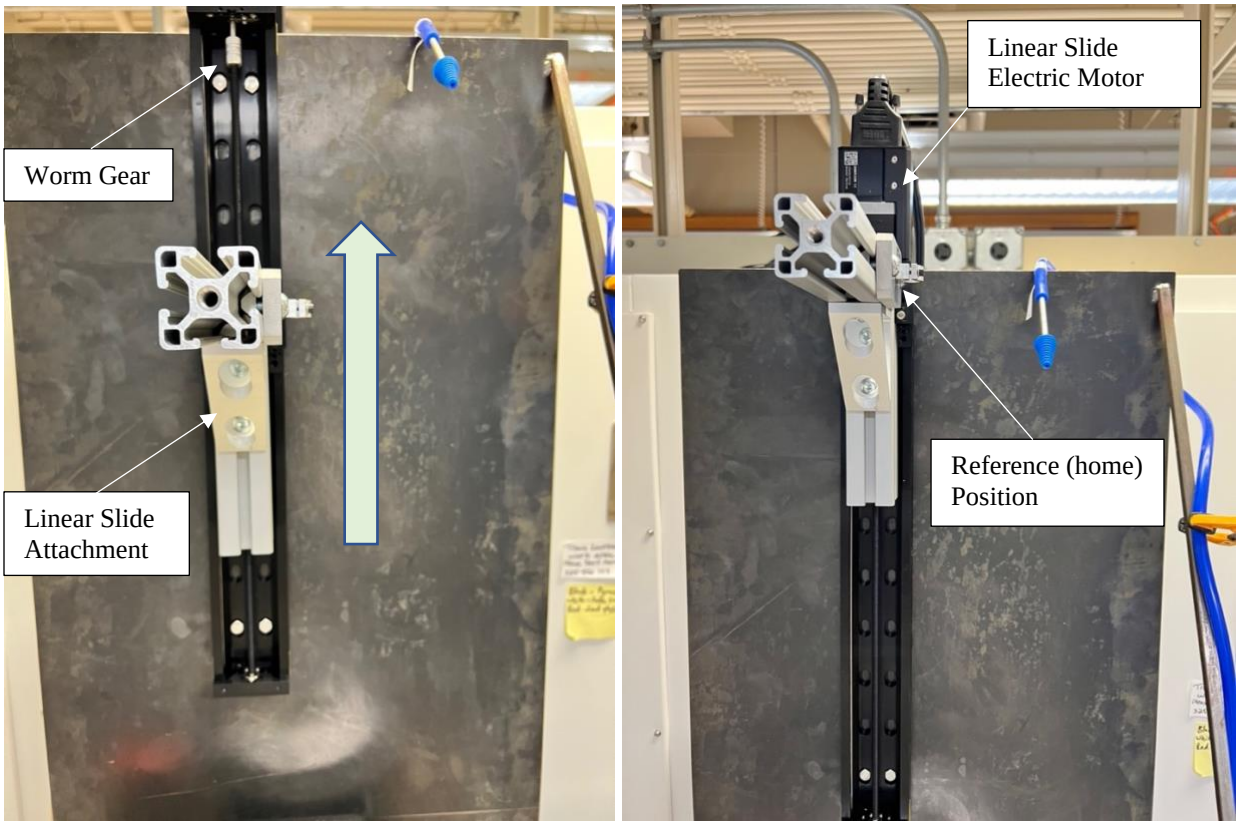

Figure 2.6- Movement of Linear Slide to Home Position

The glass tube (cladding) is prepared for mounting by wrapping electrical tape twice around the tube (720˚). In this step, it is important to ensure the electrical tape does not overlap more than once to ensure proper mounting by the tube clamp. Based on findings from misaligned tape overlap, the tube clamp will place an inconsistent force on the tube causing it to be mounted

askew and not travel centerline with the furnace. Figure 2.7 shows the prepared glass tube before and after mounting to the linear slide attachment.

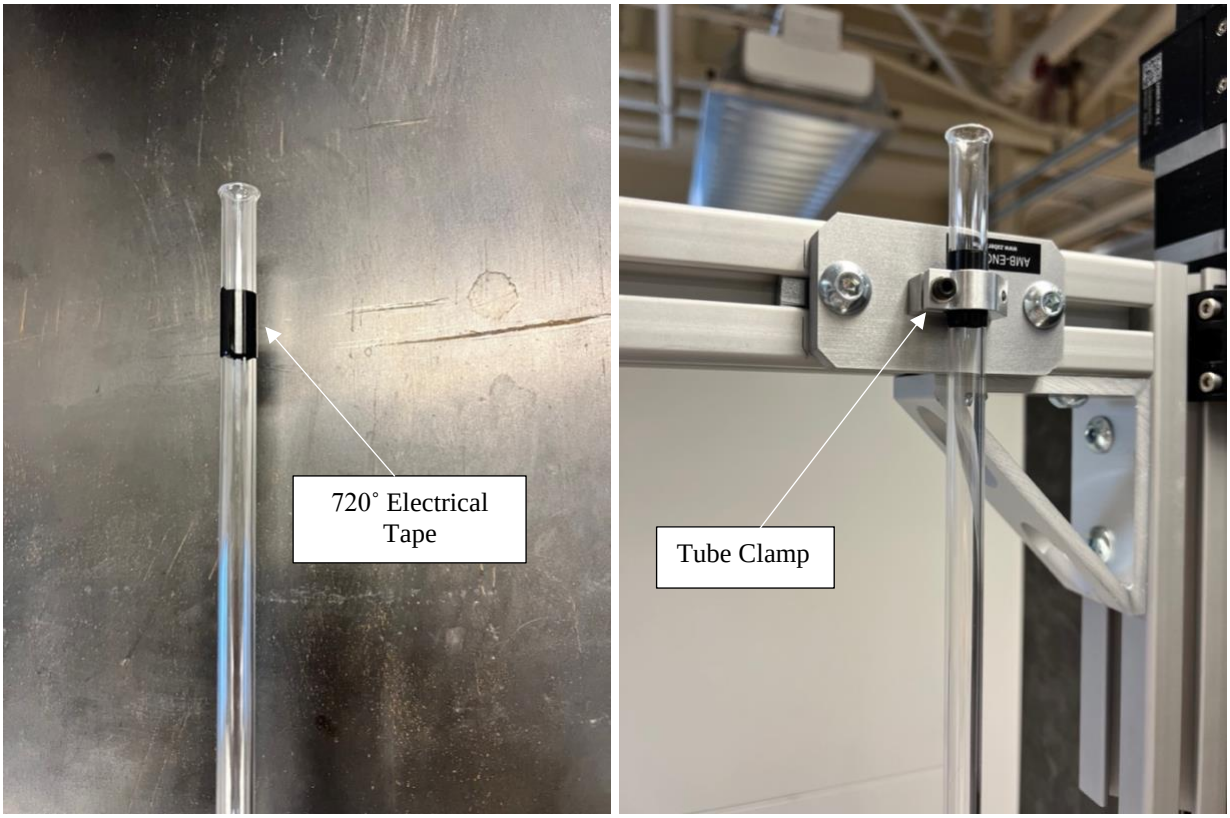

Figure 2.7- Glass Tube Before and After Mounting to Linear Slide Attachment

Once the glass tube is mounted to the downfeed assembly, the SAM 2x5 powder is poured into the top of the glass tube via a funnel to create the preform. An approximate 50 mm column on SAM 2x5 powder is shown in Figure 2.8, which is determined and discussed in the experiment section.

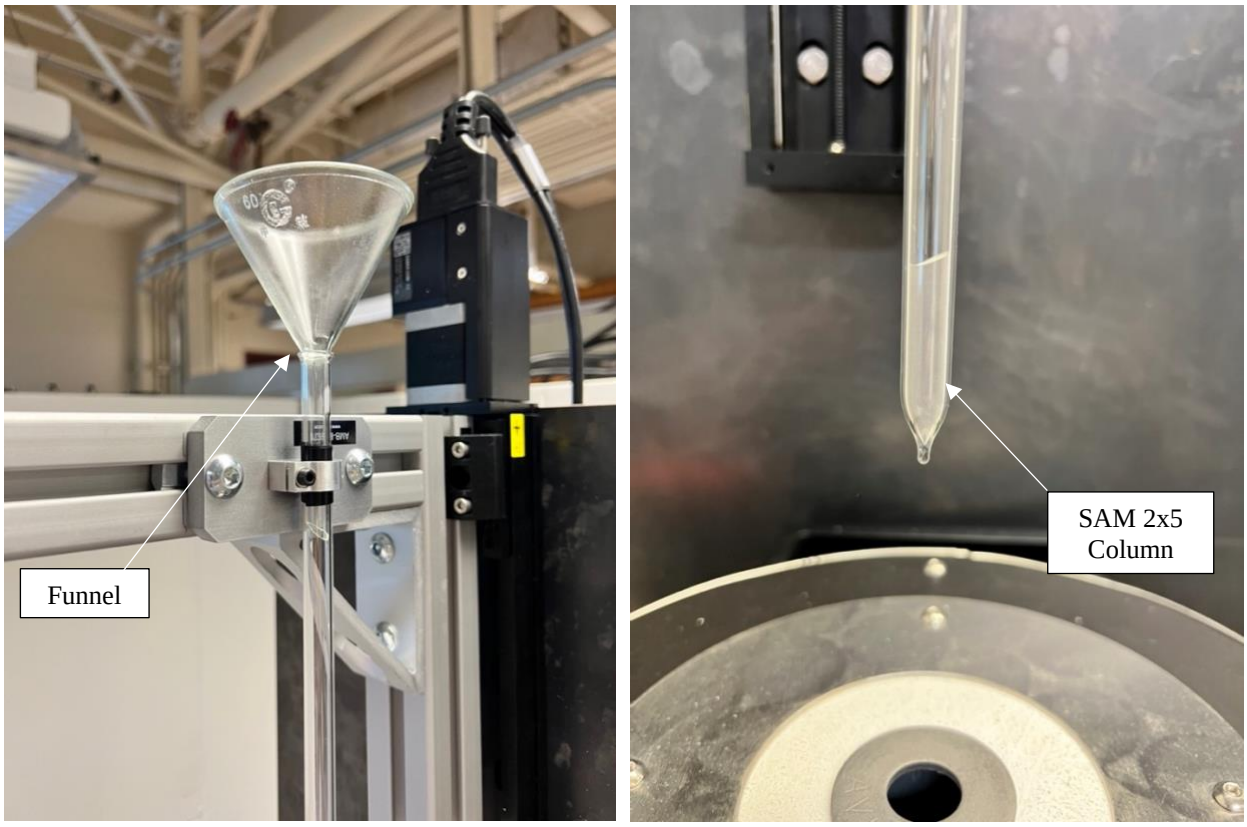

Figure 2.8- Addition of SAM 2x5 Powder to Preform

A vacuum pump is attached to the top of the glass tube after the SAM 2x5 powder is added to supply negative pressure inside the tube during the draw experiments. This negative pressure is essential to ensure the preform collapses about its centerline, allows less resistance for the SAM 2x5 column to displace upward during experiments, and inhibits oxidation of the SAM 2x5 powder once inside the furnace. The vacuum pump hose is held in position by a squeeze clamp to support the weight of the hose and not place unwanted force on the attachment. The vacuum pump attachment and assembly are shown in Figure 2.9. During experiments, the vacuum inside the glass tube reaches ~8” Hg.

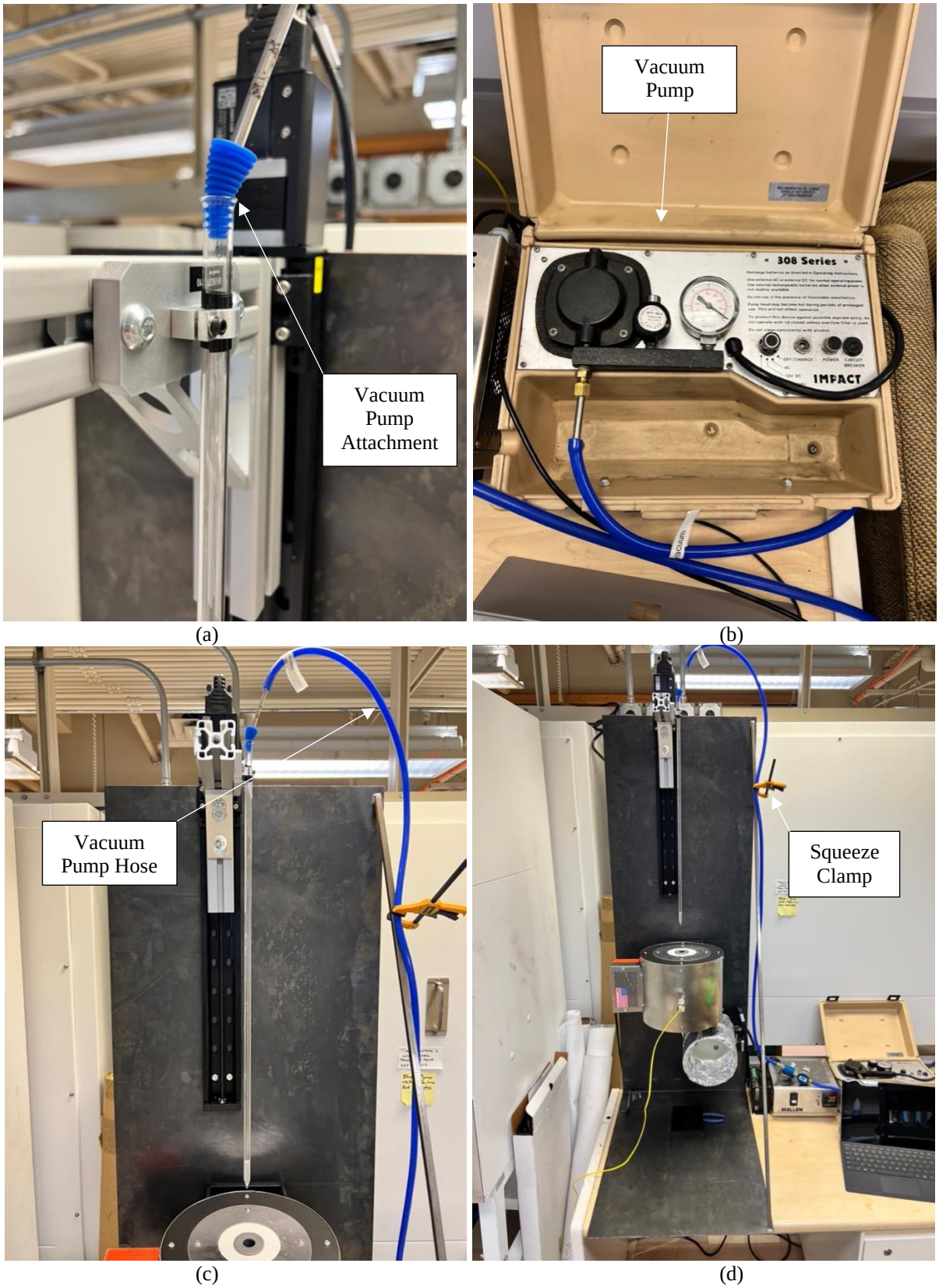

Figure 2.9- (a) Vacuum Pump Attachment to Preform, (b) Vacuum Pump, (c, d) Draw Tower Assembly with Vacuum Pump Attached to Preform

Once all prior initial conditions are met and the furnace reaches the desired temperature, the downfeed is initiated at a predetermined speed and slowly lowers the preform into the furnace. Once the top of the SAM 2x5 powder column reaches the top of the furnace, the downfeed is halted (reasoning discussed later in the experiment section) and the preform is left to soak in the furnace until gravity initiates the draw. A mirror is placed below the furnace at an angle to allow the user to safely view the preform while inside the furnace and monitor for draw initiation or issues that may arise. After the draw is initiated, the fiber exits the bottom of the furnace and is wrapped around the capstan at a predetermined speed based on the reduction ratio and equation (1). This process is shown in Figure 2.10.

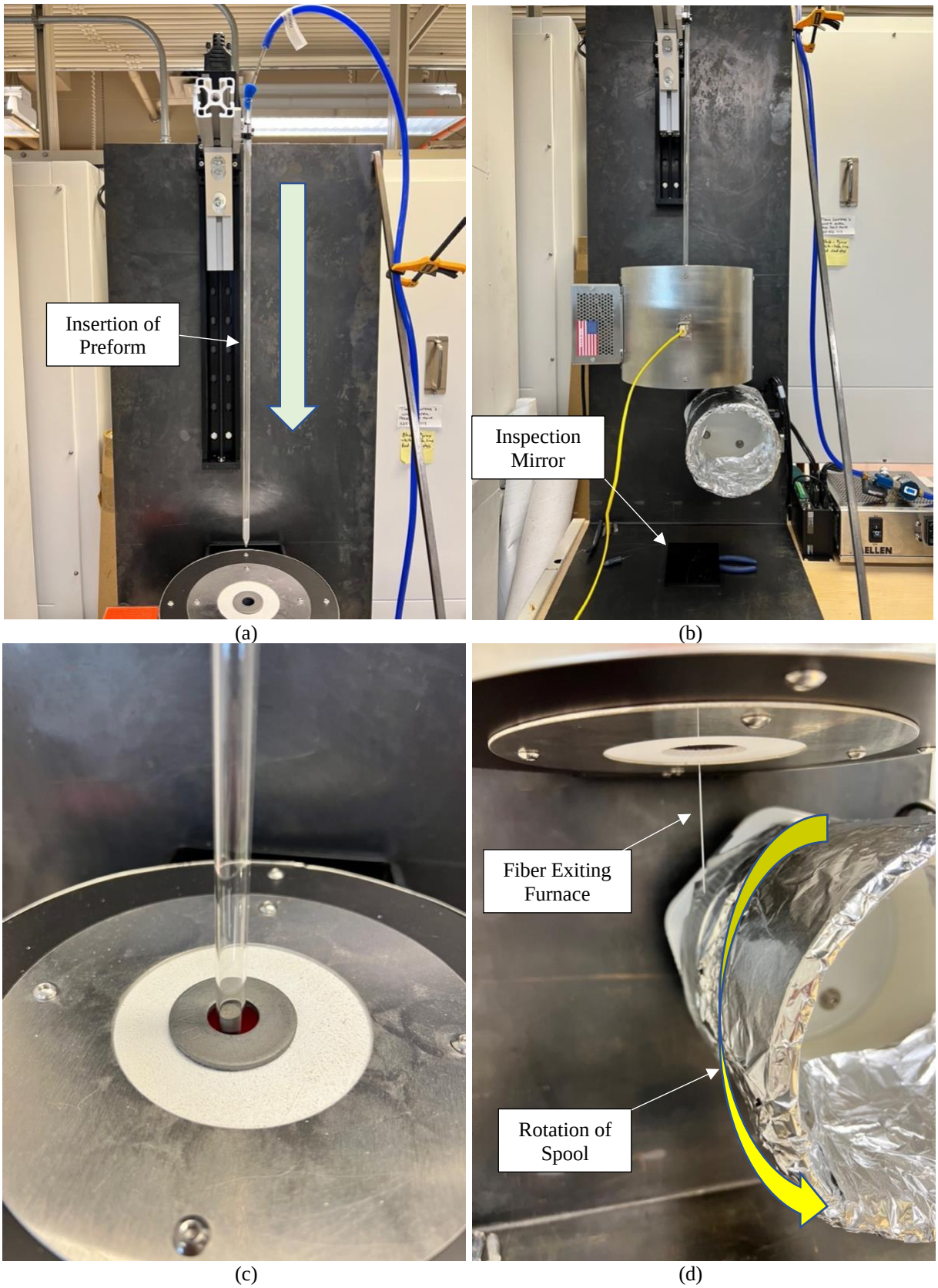

(a) (b) (c) (d)

Figure 2.10- (a) Insertion of Preform into Furnace, (b-c) Preform Halted as SAM 2x5 Powder Column Reached Top of Furnace, (d) Fiber Exiting Furnace

CHAPTER 3- EXPERIMENT

3.1- Pre-powder Experimental Section

This section is provided to show the experiments performed to test the draw tower's functionality before including the SAM 2x5 powder. During these experiments, three different types of glass (Lead Glass, Soda Lime Glass, and Borosilicate Glass) were attempted to be drawn into a fiber. After each attempt, various parameters were adjusted based on the findings and conclusion of that experiment. It is worth noting that in this section, the inner portion of the tube is hollow which affects the conservation of mass assumed in equation (1). The O.D. of the tube is 10.23 mm and the I.D. is 7.58 mm. This results in an initial area of 37.07 mm^2 and an initial simulated diameter of 6.87 mm when accounting for the lack of material in the center of the tube. Equation (1) is still relevant when attempting to determine downfeed and spool velocities, however it results in a reduction ratio of 24 compared to the target 50 that will be attempted in section 3.2.

3.1.1- Drawing Borosilicate Glass Tube at 850℃

This experiment was conducted as an initial operational test for the draw tower. A 60 cm borosilicate preform was mounted to the downfeed using 720˚ of electrical tape as cushion for the mounting bracket. The furnace was preheated to 850°C and a vacuum pump was attached to the top/open end of the tube to provide negative pressure (~8" Hg) during the draw. Once the initial conditions were set, the downfeed and capstan were initiated, moving at a speed of 100 µm/sec and 0.05 rad/sec respectively. Once the tube exited the bottom of the furnace, the draw was attempted to be manually initiated by using a pair of needle-nose pliers to create a downward force on the preform. However, the borosilicate glass was very brittle and did not

deform as expected. The preform was backed out of the furnace and returned to its initial starting position at the top of the linear slide for inspection. After the glass tube was evaluated, it was noted that a small amount of collapse occurred 1.5” from the bottom of the tube due to the negative pressure applied. Based on the lack of workability exhibited by the borosilicate tube, the furnace needed to be at a higher temperature to achieve the desired response.

3.1.2- Drawing Borosilicate Glass Tube at 900℃

This experiment was conducted as a follow-on operational test for the draw tower, increasing the furnace temperature from 850˚C to 900˚C. All other conditions were held constant. Once the initial conditions were set, the downfeed and rotating spool were initiated. The tube exited the bottom of the furnace, and the draw was again attempted to be manually initiated by using a pair of needle-nose pliers to create a downward force on the preform. However, the borosilicate glass was still far too brittle and did not neck down as expected. The preform was backed out of the furnace and returned to its initial starting position at the top of the linear slide. The glass tube had fully collapsed in on itself leaving a flattened portion 5.5” long, corresponding to the portion of the tube within the heated length of the furnace. Since 900˚C is the maximum temperature this tubular furnace can achieve, it was determined that borosilicate glass did not contain the appropriate thermal properties to achieve fibrous material based on the limiting conditions of the furnace.

3.1.3- Drawing Lead Glass Tube at 700℃

Since the borosilicate glass was unable to achieve the desired response due to its thermal properties and experimental limiting factors, lead glass was attempted to be drawn. This experiment was conducted as a starting point to observe the mechanical characteristics of lead

glass under similar conditions as borosilicate glass. Lead glass has a softening temperature of 630˚C [38], so the furnace was preheated to 700˚C. All other initial conditions were held constant. The lead glass tube was mounted to the downfeed described in section 2.8. Once the furnace temperature stabilized at 700˚C, the downfeed and rotating spool were initiated. As the lead glass exited the bottom of the furnace, the draw was attempted to be manually initiated in the same fashion as before.

Similar results to the borosilicate glass experiments were observed. The lead glass was far too brittle to deform and did not neck down into a fiber as desired. The preform was returned to its starting position at the top of the linear slide and the lead glass tube was examined. The tube did collapse into a flattened specimen roughly 1.5” from the bottom of the preform and spanned 5” in length due to the negative pressure applied. This observation showed that the temperature of the furnace needed to be raised in order to achieve a workable material and reduction in size.

3.1.4- Drawing Lead Glass Tube at 800℃

Based on the previous findings for lead glass, the furnace temperature was raised from 700˚C to 800˚C to test the concluding remarks of section 3.1.3. All other initial conditions and parameters were held constant. The downfeed and rotating spool were initiated, and the lead glass tube entered the furnace. As the tube was moving through the furnace, continuous tube collapse was observed using the inspection mirror at the base of the draw tower. Once the tube exited the bottom of the furnace, an external downward force was placed of the preform. A portion of the tube still inside of the furnace began to neck down into a fiber, approximately 3” from the bottom of the furnace. The external force was held constant, and the tube continued to neck down. Once the fibrous portion of the tube exited the bottom of the furnace, it was

attempted to be wrapped around the capstan to initiate a continuous process. However, the fibrous material had cooled and became too brittle to deform around the spool. This caused the fiber to continuously break into small pieces as it was pulled by the capstan. The results of this experiment are displayed in Figure 3.1.

Based on the rapid cooling of the fiber after it left the furnace, the furnace temperature needed to be raised to allow the exiting temperature of the fiber to be higher and stay workable for a longer period. Additionally, the speed of the downfeed and the capstan could be increased respectively using equation (1) to have the fiber spend less time between the bottom of the furnace and the capstan. In order to better determine the results of varying parameters, the furnace temperature would be adjusted first and the speeds left constant.

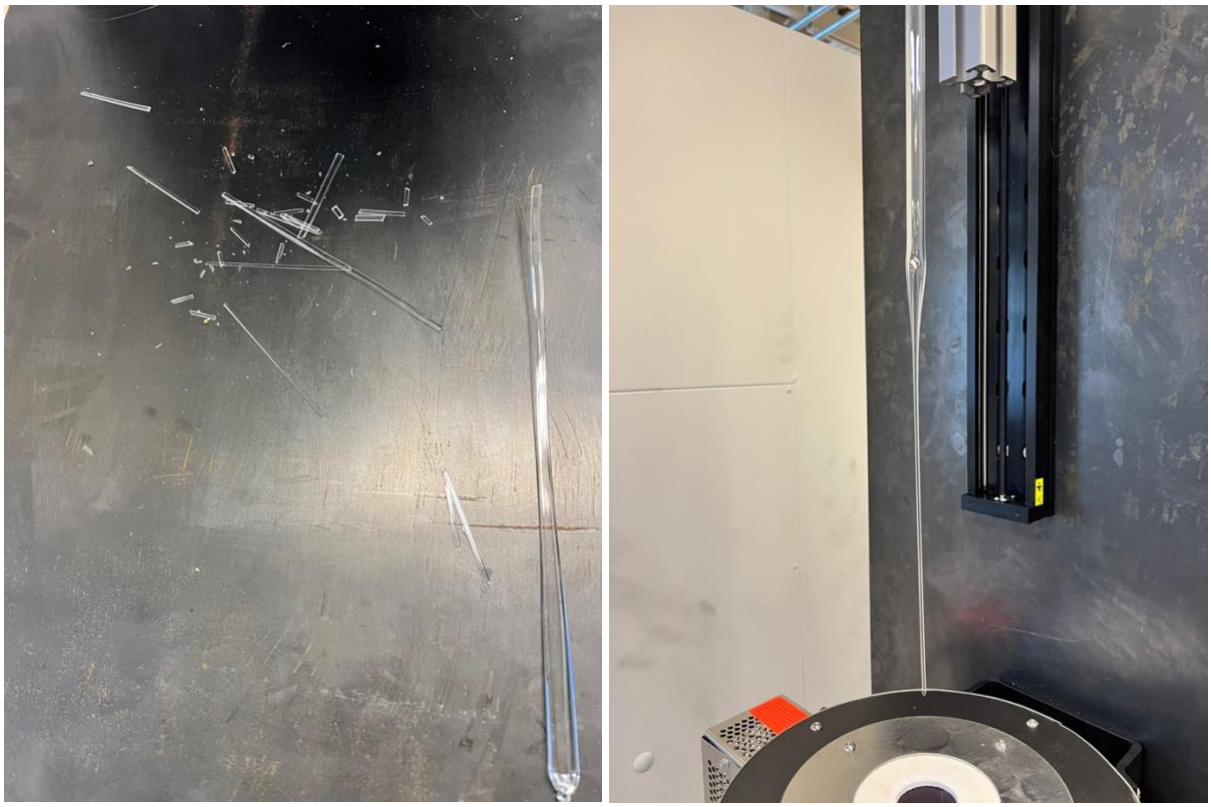

Figure 3.1- Post Experiment Lead Glass Draw 800˚C

Additionally, this experiment allowed a change of course to reevaluate using pre-sintered SAM 2x5 specimens as the core of the preform in section 3.2. Based on the observed collapse and downward force required to initiate the draw, it was determined that it would be better suited to use SAM 2x5 powder as the core of the preform versus pre-sintered specimens. The forces required to neck down the glass cladding would not be high enough to deform a pre-sintered SAM 2x5 specimen, and the specimen would simply pass through the center of the furnace unchanged. Starting with SAM 2x5 powder would allow the powder to become entrapped in the center of the tube during the collapse and sinter into a solid fiber using the heat of the furnace.

3.1.5- Drawing Lead Glass Tube at 870℃

The furnace temperature was raised from 800˚C to 870˚C to attempt to achieve a workable fiber that can be wrapped around the capstan. In order to better maintain the heat inside the furnace, a 5/8” I.D. washer was placed over the top of the furnace to reduce the chimney effect and ensure the glass was reaching the desired temperature during the draw. All other initial conditions were held constant. The downfeed and rotating spool were initiated, and the lead glass tube entered the furnace. As the tube was passing through the center of the furnace the glass began to neck down into a fiber via gravity, so manual initiation of the fiber draw process was not necessary due to the increased heat of the furnace. Once the glass fiber exited the bottom of the furnace, it was attempted to be wrapped around the capstan. The fiber was able to wrap 270˚ around the capstan before it began breaking due to cooling and becoming brittle. Wrapping the glass fiber around the spool was attempted several times with similar results. The experiment was halted and the preform was backed out of the furnace to its initial position at the top of the linear slide.

Based on the results from this experiment and section 3.1.4, it was determined that the speeds of the downfeed and capstan needed to be faster, allowing the fiber to spend less time exposed to ambient temperature before it is attempted to be wrapped around the spool. This will permit the fiber to maintain a higher temperature and its ductility as it is attempted to be collected. However, before attempting to alter the process speeds, soda lime glass was drawn to determine if better results would be obtained based on the material used.

3.1.6- Drawing Soda Lime Glass at 800℃

This experiment was performed to determine if the type of glass used to generate fibers would make a difference when the fiber was attempted to be wrapped around the capstan. The furnace was preheated to 800˚C based on soda lime glass having a softening temperature of 720˚C.[37] All other initial conditions were held constant. The downfeed and spool were initiated, and the soda lime glass tube entered the furnace. As the glass tube was progressing through the furnace, the tube began collapsing in on itself due to negative pressure applied, observed through the inspection mirror. Once the preform exited the bottom of the furnace, the draw was manually initiated, and the tube began to neck down inside the furnace. The fiber was wrapped around the capstan, however continuous fracturing was again observed. The experiment was halted after several attempts and the preform was returned to the top of the linear slide. The conclusion from this experiment was the same as section 3.1.4, the material needed to be hotter to maintain its ductility as it is wrapped around the capstan.

3.1.7- Drawing Soda Lime Glass at 880℃

This experiment was performed to test the conclusion of section 3.1.6. Based on those findings, the furnace temperature was raised from 800˚C to 880˚C. All other initial conditions

were held constant. The same soda lime glass tube from section 3.1.6 was used, so there was already a preformed fiber present at the tip of the tube, allowing a convenient access point to manually initiate the draw if necessary. The downfeed and rotating spool were initiated, and the glass tube entered the furnace. As the fiber exited the furnace, the draw was manually initiated/continued. The fiber was more workable when attempted to be wrapped around the capstan, but the same issues were encountered. The glass fiber stayed intact for a longer duration but broke continuously before reaching a complete revolution.

Since the furnace was close to its maximum temperature, it was apparent that the speeds of the downfeed and capstan needed to be increased, permitting the fiber to spend less time exposed to ambient temperature before being collected on the capstan.

3.1.8- Drawing Soda Lime Glass at 900℃, Increase in Downfeed and Spool Speed

This experiment was performed to determine if increasing the relative speeds of the downfeed and rotating spool would allow the glass fiber to maintain its ductility long enough to wrap around the capstan without fracturing and create a continuous process. The downfeed was chosen to descend at 300 μm/sec (3x faster than before), resulting in the drum rotating at 0.17 rad/sec based on a reduction ratio of 24 and equation (1). The same soda lime glass tube was reused, so again there was a preformed fiber located at the tip of the tube. The furnace was preheated to its maximum temperature of 900˚C and all other initial conditions were held constant. The downfeed and rotating spool were initiated, and the soda lime glass tube entered the furnace. As the tube was proceeding through the furnace, the draw was initiated via gravity midway through. As the fiber was descending to the bottom of the furnace, the fiber began to sway and became affixed to the inner wall of the furnace. This caused the remaining fiber to start bunching up inside the furnace due to the blockage. The experiment was aborted, and the soda

lime tube was returned to the top of the linear slide. The bunched glass and furnace were allowed to cool for several hours before attempting to clear the now solidified glass blockage from the center of the furnace.

Once the glass was cleared, the same initial conditions were established and the experiment was attempted again, since it was not clear why the glass had affixed itself to the side of the furnace. However, the same results were obtained; the glass fiber affixed itself to the furnace wall for a second time, causing another blockage and aborted experiment. Based on these findings it was determined that the furnace was too hot, causing the soda lime glass to develop a liquid exterior and affix to the inner wall of the furnace when contacted. The fiber was swaying inside the furnace, contacting the inner wall, due to increased ductility which was heavily influenced by the temperature gradients inside the furnace. Additionally, based on the ease of which soda lime glass was sticking to the inner wall of the furnace, it was concluded that lead glass was better suited for this application and to continue with the findings from section 3.1.5.

3.1.9- Drawing Lead Glass at 870℃, Increase in Downfeed and Spool Speed

The findings determined in section 3.1.5 and 3.1.7 showed that the downfeed and capstan velocities needed to be increased. While attempting the soda lime glass experiments, the speeds were increased by a factor of 3. Even though the new speeds were never fully tested based on other complications, it was apparent to the team that the process was still too slow. In this experiment, the capstan was chosen to rotate at 0.3 rad/sec based on trialing various speeds and determining this reasonable based on the data observed so far. Using equation (1), this resulted in the downfeed moving at 501 µm/sec using a reduction ratio of 24. The furnace was preheated to 870˚C and all other initial conditions were held constant. As the lead glass preform progressed

through the furnace, the draw was initiated via gravity. Once the fiber exited the bottom of the furnace, the fiber was attempted to be wrapped around the capstan.

Due to the increased proportion in speeds of the downfeed and the spool, a continuous process was achieved, and the fiber was able to be collected around the capstan for four revolutions before the experiment was stopped in order to conserve glass. The glass fiber was cut at the bottom of the furnace to allow safe withdraw of the preform and to allow a pre-drawn fiber to be used in the SAM 2x5 powder section. The preform was returned to its starting position at the top of the linear slide. Once the glass fiber was cut, the glass collected around the capstan unwound due to loss of tension and expectedly broke into 4 large pieces, shown in Figure 3.2.

This experiment showed that a continuous process was viable with the correct parameters in place. These parameters would be used to begin the experiments with SAM 2x5 powder in the center of the glass tubes.

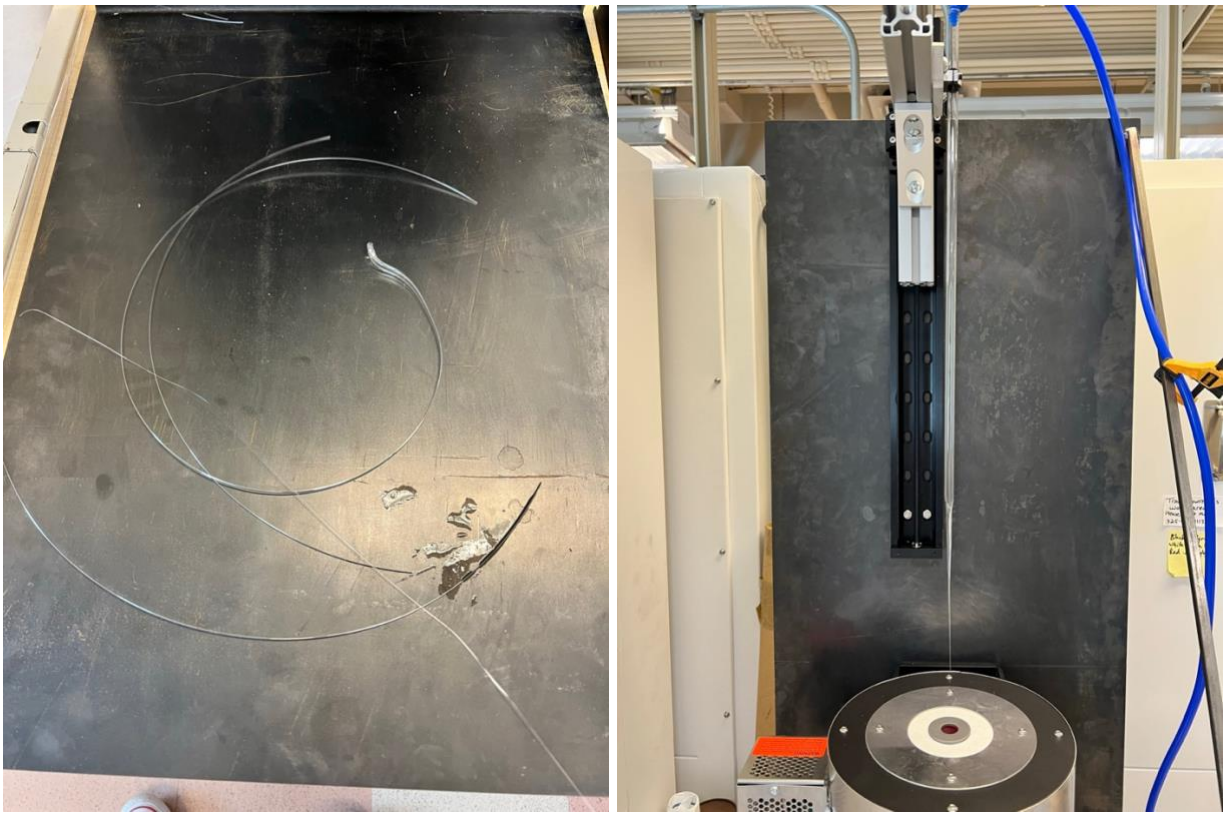

Figure 3.2- Post Experiment Lead Glass Draw 870˚C, Increased Downfeed and Spool Velocities

3.2- SAM 2x5 Powder Experimental Section

This section is provided to show the experiments performed while including the SAM 2x5 powder as the core of the preform. During these experiments, only lead glass cladding with a SAM 2x5 powder core was attempted to be drawn into a fiber based on results from section 3.1. After each attempt, various parameters were adjusted based on the findings and conclusion from that experiment.

3.2.1- Drawing Lead Glass at 870℃ with 130mm SAM 2x5 Powder

This experiment was conducted as an operational test of the draw tower with a preform containing a 130 mm column of SAM 2x5 powder. The same lead glass tube from section 3.1.9 was utilized in this experiment due to already having a fibrous portion present at the tip of the

tube, allowing the draw to be manually initiated if necessary. A funnel was used to add the SAM 2x5 powder into the center of the tube, described in section 2.8. The initial preform is shown in Figure 3.3. The furnace was preheated to 870°C and a vacuum pump was attached to the top/open end of the tube to provide negative pressure (~8" Hg) during the draw. Once the initial conditions were set, the downfeed and rotating spool were initiated, moving at a speed of 501 µm/sec and 0.3 rad/sec respectively based on the findings from section 3.1.9. The center of the tube was now filled with SAM 2x5 powder, causing the reduction ratio to change from 24 to 50, based on conservation of mass equation (1).

Figure 3.3- Initial Preform with 130 mm SAM 2x5 Powder

Once the initial conditions were set, the downfeed and rotating spool were initiated. As the preform moved through the furnace, the preestablished fiber continued to neck down as expected. The end of the fiber exited the bottom of the furnace and was attempted to be wrapped around the capstan. As the fiber continued to exit the bottom of the furnace, small pieces of SAM 2x5 began to appear, shown in Figure 3.4. As the process continued, the fiber diameter started to decrease significantly with fewer pieces of SAM 2x5 present. Roughly one minute after initiation of the experiment, the remaining SAM 2x5 powder portion of the preform fell to the bottom of the furnace, shown in Figure 3.5. The experiment was stopped, and the remaining preform was returned to the top of the linear slide.

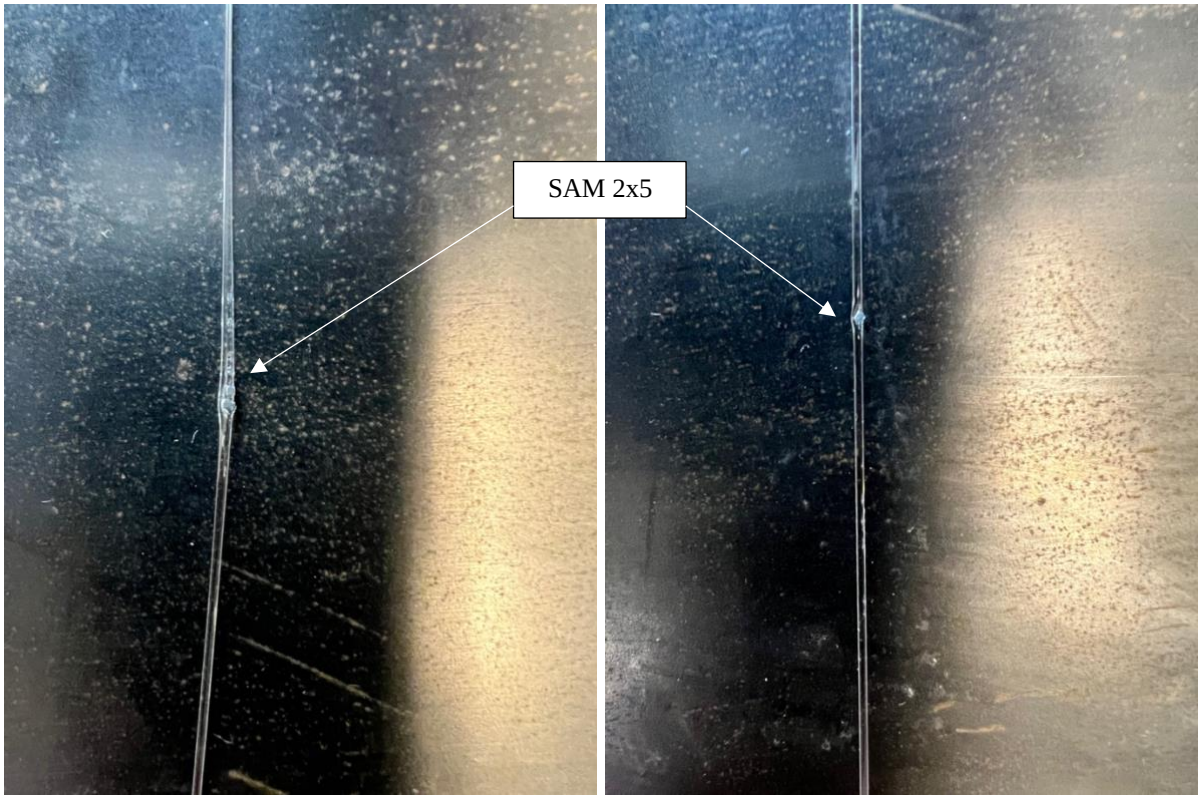

Figure 3.4- Small Pieces of SAM 2x5 in Fiber

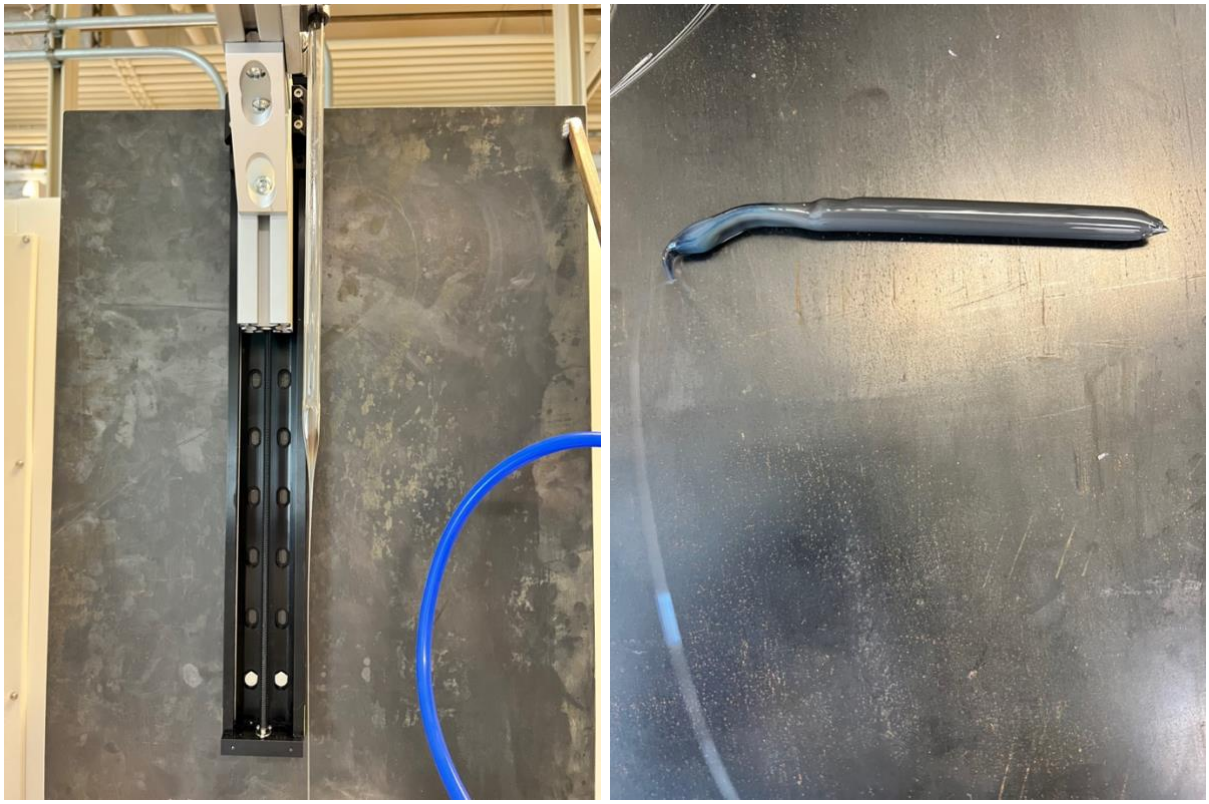

Figure 3.5- Post Experiment Preform

During post experiment analysis, it was determined that the large section of SAM 2x5 fell to the bottom of the furnace due to the hollow section of the preform above the SAM 2x5 powder line entering the furnace. This allowed the hollow section of the preform to create a second neck down region and caused the SAM 2x5 powder region to fall. Additionally, there was too much SAM 2x5 powder in the preform to begin with. Since the preform is reducing in size during the fiber draw process, the remaining SAM 2x5 powder column is required to displace toward the top of the preform. The small force being applied to the bottom of the column during reduction was not enough to overcome the weight of the 130 mm column of SAM 2x5 powder and displace it upward. This was another contributing factor as to why the powder did not cohesively draw with the surrounding glass cladding. These conclusions will be applied in the following sections.

Lastly, the post experiment SAM 2x5 preform was analyzed to determine how the heat of the furnace affected the SAM 2x5 powder. Figure 3.6 shows the SAM 2x5 section which was cut to determine if the heat of the furnace was enough to cause the powder to densify or if it would remain in its powderous form. Upon analysis, the SAM 2x5 core did form a loosely packed solid. This shows that the heat of the furnace is enough to sinter the powder together, allowing the basis for using powder as the core of the preform to continue.

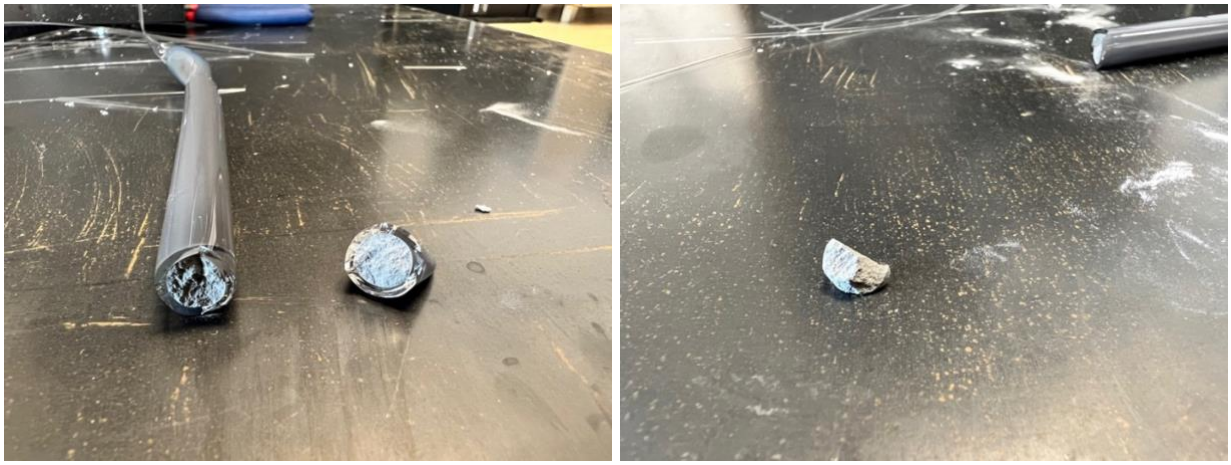

Figure 3.6- Post Experiment SAM 2x5 Solid

3.2.2- Drawing Lead Glass at 870℃ with 15mm SAM 2x5 Powder

From the findings of section 3.2.1, this experiment was performed with 88.5% less SAM 2x5 powder, which should allow the powder column to displace upward during the draw process. The initial starting preform is shown in Figure 3.7. All other initial conditions were held constant. The downfeed and rotating spool were initiated, however the downfeed was stopped as the top of the SAM 2x5 powder column reached the top of the furnace. This would prevent a second neck down region from occurring above the powder column, as seen in the previous experiment. Once the preform reached its holding point, the draw initiated itself via gravity. As

the fiber was being drawn, the SAM 2x5 powder column was visibly moving up the remaining tube due to the reduction occurring inside the furnace. This validated the conclusion determined in section 3.2.1 that excessive powder was used initially, which prevented the column from displacing.

Figure 3.7- Initial Preform with 15mm SAM 2x5 Powder

As the draw was occurring, small pieces of SAM 2x5 were entrapped inside the glass fiber in the same manner as section 3.2.1. As the draw continued, the fiber diameter began to rapidly shrink, causing the fiber generation to be interrupted. Additionally, since this preform had been used in two prior experiments, the downfeed had reached the end of the track and the

preform could not further descend into the furnace. This caused the experiment to stop based on lack of fiber generation and loss of downfeed. The remaining preform was returned to the top of the linear slide and the post experiment specimen was examined to note any differences from the findings of section 3.2.1. The post experiment preform is shown in Figure 3.8.

Figure 3.8- Post Experiment Preform

Although the preform reached the end of the linear slide track causing the experiment to end, the results of this experiment showed marked improvement from section 3.2.1. The preform was able to deform into a semi-flat specimen with the SAM 2x5 powder entrapped in the center from the heat of the furnace and the negative pressure applied from the vacuum pump. This deformation was accomplished by the powder column having the ability to displace toward the top of the tube and by preventing the entire powder column from entering the furnace. This

verifies the findings from section 3.2.1 and will be continued on the next experiment, starting with a new preform.

3.2.3- Drawing Lead Glass at 870℃ with 50mm SAM 2x5 Powder

This experiment was performed as a continuation from section 3.2.2. A new lead glass preform was filled with a 50 mm column of SAM 2x5 powder. All other initial conditions were held constant. The downfeed and rotating spool were initiated, and the downfeed was stopped when the top of the powder column reached the top plane of the furnace. As the preform reached the internal temperature of the furnace, the draw was initiated via gravity. While the powder column was displacing due to the reduction occurring inside the furnace, the preform was continued to be lowered to keep the top of the powder column even with the top plane of the furnace.

While the draw continued, small pieces of SAM 2x5 were noted in the glass fibers being formed. The longer the process was maintained, larger sections of the fibers being generated were filled with SAM 2x5. At the end of the experiment, a fiber 180 mm long and ~0.3 mm in diameter was generated, containing significant amounts of SAM 2x5. This fiber was analyzed under a Keyence VHX1100 optical microscope, and the results are displayed in Figure 3.9.

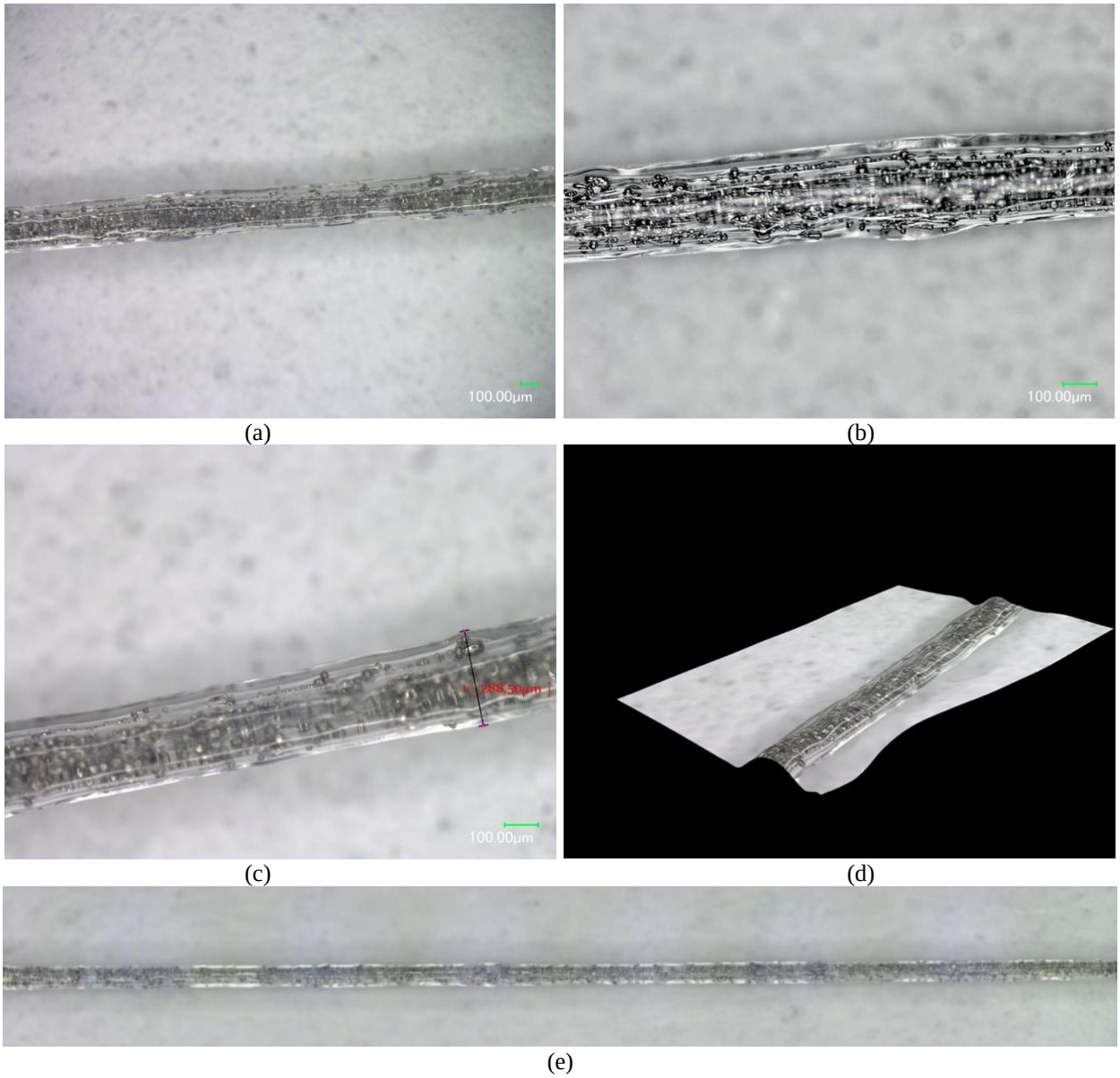

(a) (b)

(c) (d)

(e)

Figure 3.9- Optical Images of Post Experiment SAM 2x5 Fiber 870˚C. (a) 100x High Definition, (b) 200x HDR, (c) 200x Showing ~300 µm Diameter, (d) 3D Render of Fiber, (e) 100x Stitched Image

Based on post experiment observation, the SAM 2x5 particles did not form a continuous fiber. This was caused by the SAM 2x5 powder column sintering together into a loosely packed solid prior to the neck down region where the fiber was being formed, similar to section 3.2.1. Small particles broke from the loosely packed solid SAM 2x5 column and were entrapped inside the forming lead glass fibers, resulting in discontinuous portions of SAM 2x5 particles included.

Based on these findings, this experiment would be attempted at 900˚C to determine if the elevated temperature of the SAM 2x5 powder would allow it to deform into the center of the glass cladding during the draw and form a continuous fiber.

3.2.4- Drawing Lead Glass at 900℃ with 50mm SAM 2x5 Powder

Due to the large amount of SAM 2x5 particles included in the 870˚C post draw fiber, this experiment was performed at 900˚C to determine if an elevated temperature closer to the SAM 2x5 melting point ($T_{m,\ SAM\ 2x5}$= 1200˚C)[42] would allow a continuous fiber to be generated. All other conditions were held constant. The fiber draw process was identical to section 3.2.3. However, the post experiment fiber that was generated contained significantly less SAM 2x5. The fiber was analyzed using a Keyence VHX1100 optical microscope, shown in Figure 3.10.

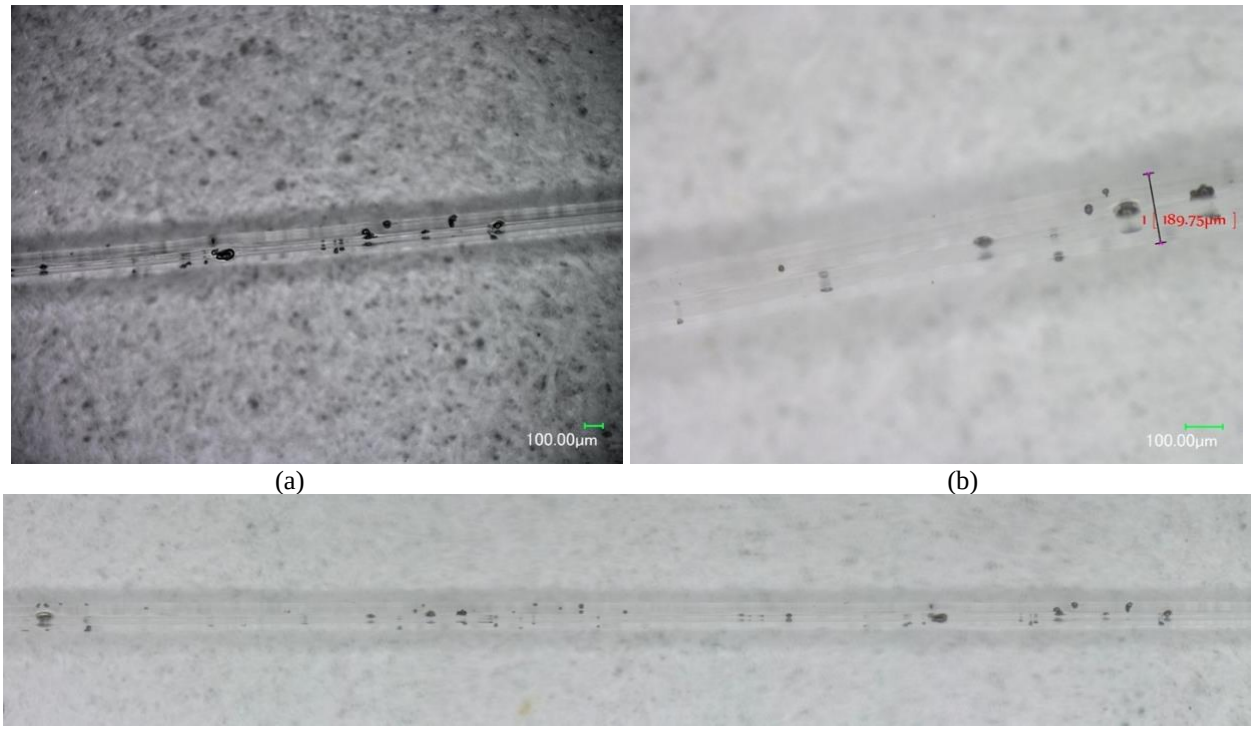

(a) (b)

(c)

Figure 3.10- Optical Images of Post Experiment SAM 2x5 Fiber 900˚C. (a) 100x HDR Image of Fiber, (b) 200x Showing Fiber Diameter, (c) 100x Stitched Image

The lack of SAM 2x5 included in this fiber was contributed to the increase in temperature. The SAM 2x5 column further solidified into a large solid column before reaching the neck down region, which prevented a large number of pieces to break off into the fiber during the draw process. This caused mainly glass cladding to be drawn with very few pieces of SAM 2x5 included. The process was unable to continue once the SAM 2x5 sintered column reached the neck down region and the experiment was stopped. Based on the further solidification of the SAM 2x5 column at 900˚C, improved results may be achieved at a lower temperature to allow the SAM 2x5 to deform with the cladding during the draw process.

3.2.5- Drawing Lead Glass at 800℃ with 50mm SAM 2x5 Powder

The high amount of SAM 2x5 particles included in section 3.2.3 and the lack of SAM 2x5 included in section 3.2.4 led to a draw attempt at 800˚C to determine if a lower temperature would allow the solidification of the SAM 2x5 column to be delayed until reaching a fibrous state. All other conditions were held constant. The fiber draw process was the same as section 3.2.3, but the results were identical to section 3.2.4. The resulting fibers contained very few pieces of SAM 2x5 (Figure 3.11), leading to the conclusion that 870˚C is an ideal draw temperature based on experimental results.

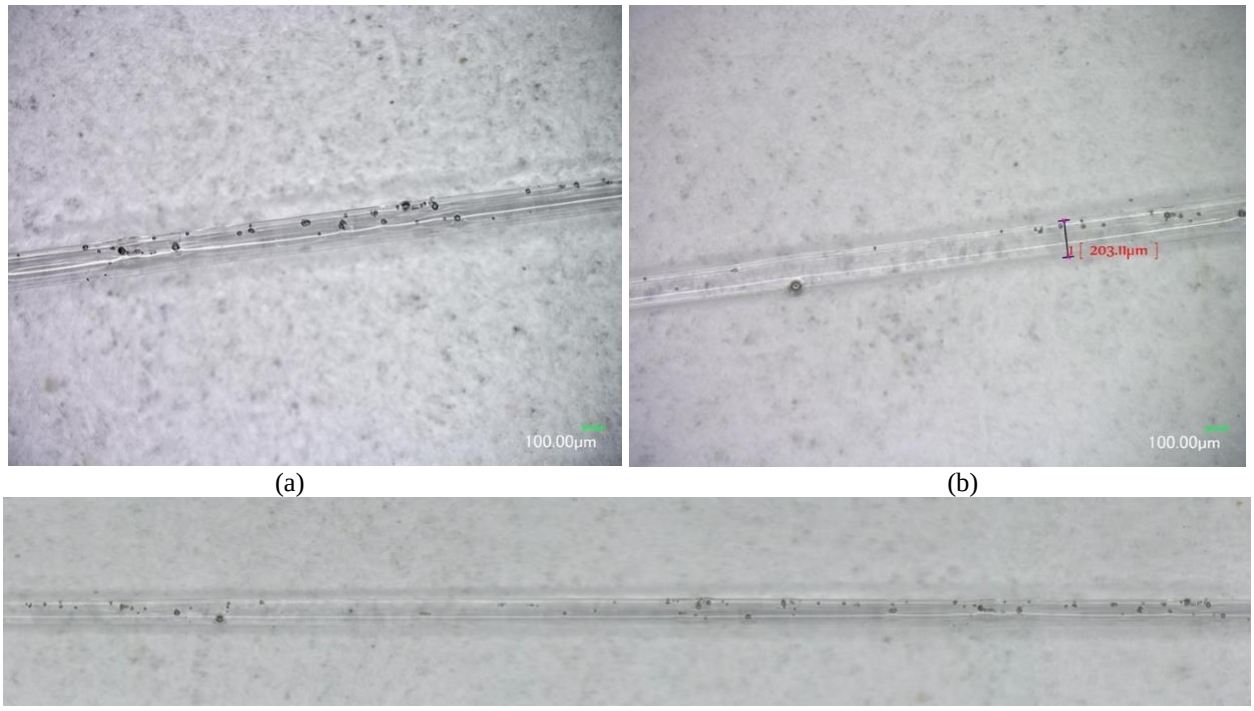

(a) (b)

(c)

Figure 3.11- Optical Images of Post Experiment SAM 2x5 Fiber 800˚C. (a) 100x HDR Image of fiber, (b) 100x Showing Fiber Diameter, (c) 100x Stitched Image

CHAPTER 4- CONCLUSION

The objective of this study was to determine if an iron-based amorphous metallic alloy ($Fe_{49.7}Cr_{17.7}Mn_{1.9}Mo_{7.4}W_{1.6}B_{15.2}C_{3.8}Si_{2.4}$) known as SAM 2x5 could deform into long continuous fibers via a thermal draw tower. Initially, the draw tower and preform design was based on using SAM 2x5 samples that had been densified via SPS. However, as experiments were conducted, the core of the preform was changed to SAM 2x5 powder to allow deformation and in situ sintering of the powder. The preform consists of SAM 2x5 powder core and a lead glass cladding to assist with the stresses that accompany the thermal draw process.

The thermal draw tower was modeled after an optical fiber draw tower, consisting of a downfeed, furnace, capstan, and a stand. All parts of the draw tower were modeled in SolidWorks to ensure relative component sizing was appropriate and create the necessary attachments to hold the preform and collect the fibers. The draw tower was assembled in house, ensuring precise measurements that would allow the preform to travel through the furnace unobstructed and eliminate any unwanted lateral forces on the fiber.

Experiments without the SAM 2x5 core in the center of the preform were ran to test the operation of the draw tower. Several iterations of the experiment were conducted with various changing parameters based on findings from the previous. A successful continuous fiber generation was obtained with lead glass cladding, furnace temperature of 870˚C, downfeed moving at 501μm/sec, capstan rotating at 0.3 rad/sec, and a vacuum pump drawing 8” Hg. Based on these results, the SAM 2x5 powder was added as the core of the preform and similar experiments were conducted to attempt to generate a continuous SAM 2x5 fiber.

When various experiments with the SAM 2x5 powder were conducted, the temperature of the furnace and the height of the SAM 2x5 powder column were the main parameters that

were adjusted. A vastly larger amount of SAM 2x5 (compared to other experiments) was able to be included in the post draw fiber with the following parameters: 50 mm column of SAM 2x5 powder, lead glass cladding, 870˚C furnace temperature, halting of the downfeed when the top of the column reached the top of the furnace, capstan rotating at 0.3 rad/sec, and 8” Hg vacuum applied to the preform. The post draw fiber was analyzed via SEM, shown in Figure 4.1.

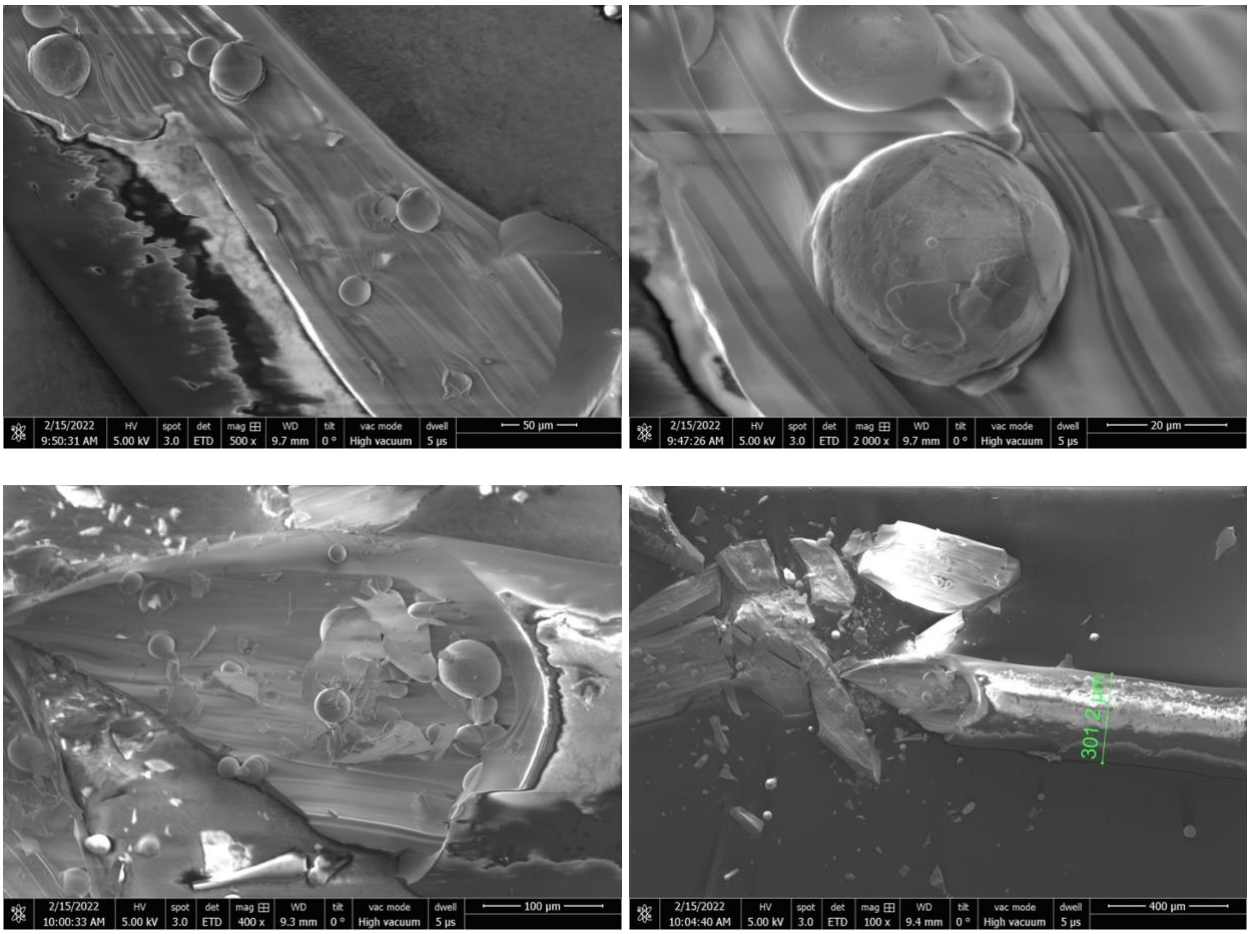

Figure 4.1- SEM images of SAM 2x5 Post Draw Fiber

Figure 4.1 shows a ~300 µm fiber which was created via the thermal draw process. However, the SAM 2x5 formed discontinuous spheres scattered throughout the glass cladding instead of a continuous fiber. A continuous fiber was not able to be generated due to the SAM 2x5 powder column solidifying from the heat of the furnace prior to the neck down portion of the draw. As the solidified powder column reached the neck down phase, the surrounding glass

cladding continued to draw into a rapidly decreasing diameter fiber. This caused the diameter of the resulting fiber to reach 300 µm, compared to the target fiber diameter of ~1 mm. The SAM 2x5 spheres were included in this fiber due to the solidified SAM 2x5 powder column producing a loosely solidified solid, shown in section 3.2.1. Since this powder column is very loosely densified, as the surrounding glass cladding continued to be drawn into a fiber, spherical pieces of the SAM 2x5 column broke off and were included in the resulting fiber.

The amount of SAM 2x5 included in the fiber varied largely based on temperature. Significantly less SAM 2x5 was included in the experiments conducted at 800˚C and 900˚C. At 800˚C, the glass cladding was not hot enough to continuously draw around the SAM 2x5 powder column, which caused the glass cladding to break and discontinue the draw process as the SAM 2x5 powder column reached the neck down region. At 900˚C, the increase in temperature caused the SAM 2x5 powder column to further solidify. This caused the column to resist breaking as the glass cladding around the column continued to draw, resulting in fewer SAM 2x5 particles included in the post draw fiber.

For future work, if the SAM 2x5 powder is continued to be used as the core of the preform, the core to cladding ratio should be changed. The glass cladding makes up 5.3 mm of the preform cross-section, compared to the 7.58 mm of the SAM 2x5 powder. If the glass cladding encompassed more of this cross-section and the powder column was not as thick, the SAM 2x5 powder column may deform into a fiber based on starting with a smaller area. However, the resulting SAM 2x5 fiber would be very loosely densified and would not mimic the properties of the fully densified SAM 2x5 samples generated via SPS. While the temperature of the experiments was enough to form a loosely packed solid, the lack of pressure applied during the draw process causes the solid to be very porous and break apart easily.

Success may come from using pre-densified SAM 2x5 samples via SPS. However, based on the findings from these experiments the temperature of the process would need to be increased higher than the limitations of the furnace used. In order to allow the SAM 2x5 sintered samples to deform into a fiber, the temperature would need to approach the melting temperature of SAM 2x5 ($T_{m,\ SAM\ 2x5}$= 1200˚C).[42] However, this would cause the SAM 2x5 samples to rapidly crystalize[1] and may cause fibrous breakup.[34] Rather than reheating the SAM 2x5 sintered samples into the SCLR, an approach such as rapid quenching of a molten SAM 2x5 fiber could be used based on the thin geometry attempting to be achieved and therefore high cooling rates that would be allowed.[29] SAM 2x5 is a marginal glass former with R_c= ~600 K/min,[43,44] so a sufficiently thin fiber may bypass the crystalline barrier when cooled and achieve an amorphous fiber.

REFERENCES

(1) Graeve, O. A.; Kanakala, R.; Kaufman, L.; Sinha, K.; Wang, E.; Pearson, B.; Rojas-George, G.; Farmer, J. C. Spark Plasma Sintering of Fe-Based Structural Amorphous Metals (SAM) with Y2O3 Nanoparticle Additions. *Mater. Lett.* **2008**, *62* (17–18), 2988–2991. https://doi.org/10.1016/j.matlet.2008.01.092.

(2) Wang, W. H.; Dong, C.; Shek, C. H. Bulk Metallic Glasses. *Mater. Sci. Eng. R Reports* **2004**, *44* (2–3), 45–89. https://doi.org/10.1016/j.mser.2004.03.001.

(3) Graeve, Olivia. "Amorphous Metals." Structure and Analysis of Solids. Lecture 8 of MATS 227, Oct. 2020, La Jolla, UCSD.

(4) Klement, W.; Willens, R. H.; Duwez, P. Non-Crystalline Structure in Solidified Gold-Silicon Alloys. *Nature* **1960**, *187* (4740), 869–870. https://doi.org/https://doi.org/10.1038/187869b0.

(5) Greer, A. L. Metallic Glasses. *Science* **1995**, *267*, 1947. https://doi.org/doi.org/10.1126/science.267.5206.1947.

(6) Johnson, W. L. Thermodynamic and Kinetic Aspects of the Crystal to Glass Transformation in Metallic Materials. *Prog. Mater. Sci.* **1986**, *30* (2), 81–134. https://doi.org/10.1016/0079-6425(86)90005-8.

(7) Jafary-Zadeh, M.; Kumar, G. P.; Branicio, P. S.; Seifi, M.; Lewandowski, J. J.; Cui, F. A Critical Review on Metallic Glasses as Structural Materials for Cardiovascular Stent Applications. *J. Funct. Biomater.* **2018**, *9* (1), 1–32. https://doi.org/10.3390/jfb9010019.

(8) Busch, R. Thermophysical Properties of Bulk Metallic Glass-Forming Liquids. *Jom* **2000**, *52* (7), 39–42. https://doi.org/10.1007/s11837-000-0160-7.

(9) Inoue, A.; Zhang, T.; Masumoto, T. Glass-Forming Ability of Alloys. *J. Non. Cryst. Solids* **1993**, *156–158* (PART 2), 473–480. https://doi.org/10.1016/0022-3093(93)90003-G.

(10) Greer, A. L. Metallic Glasses...on the Threshold. *Mater. Today* **2009**, *12* (1–2), 14–22. https://doi.org/10.1016/S1369-7021(09)70037-9.

(11) Johnson, W. L.; Samwer, K. A Universal Criterion for Plastic Yielding of Metallic Glasses with a (T/Tg)2/3 Temperature Dependence. *Phys. Rev. Lett.* **2005**, *95* (19), 2–5. https://doi.org/10.1103/PhysRevLett.95.195501.

(12) Ashby, M. F.; Greer, A. L. Metallic Glasses as Structural Materials. *Scr. Mater.* **2006**, *54* (3), 321–326. https://doi.org/10.1016/j.scriptamat.2005.09.051.

(13) Takeuchi, S.; Edagawa, K. Atomistic Simulation and Modeling of Localized Shear Deformation in Metallic Glasses. *Prog. Mater. Sci.* **2011**, *56* (6), 785–816. https://doi.org/10.1016/j.pmatsci.2011.01.007.

(14) Greer, A. L.; Cheng, Y. Q.; Ma, E. Shear Bands in Metallic Glasses. *Mater. Sci. Eng. R Reports* **2013**, *74* (4), 71–132. https://doi.org/10.1016/j.mser.2013.04.001.

(15) Limthongkul, P.; Jang, Y.-I.; Dudney, N. J.; Chiang, Y.-M. Electrochemically-Driven Solid-State Amorphization in Lithium-Silicon Alloys and Implications for Lithium Storage. *Acta Mater.* **2003**, *51* (4), 1103–1113. https://doi.org/10.1016/S1359-6454(02)00514-1.

(16) Rehn, L. E.; Okamoto, P. R.; Pearson, J.; Bhadra, R.; Grimsditch, M. Solid-State Amorphization of Zr3Al: Evidence of an Elastic Instability and First-Order Phase Transformation. *Phys. Rev. Lett.* **1987**, *59* (26), 2987–2990. https://doi.org/10.1103/PhysRevLett.59.2987.

(17) Chukalkin, Y. G.; Goshchitskii, B. N. Radiation Amorphization of Orthoferrite YFeO3. *Phys. Status Solidi* **2003**, *200* (2), R9–R11. https://doi.org/10.1002/pssa.200309020.

(18) Shimizu, F.; Ogata, S.; Li, J. Theory of Shear Banding in Metallic Glasses and Molecular Dynamics Calculations. *Mater. Trans.* **2007**, *48* (11), 2923–2927. https://doi.org/10.2320/matertrans.MJ200769.

(19) Li, Q. K.; Li, M. Atomic Scale Characterization of Shear Bands in an Amorphous Metal. *Appl. Phys. Lett.* **2006**, *88* (24), 1–4. https://doi.org/10.1063/1.2212059.

(20) Li, Q. K.; Li, M. Assessing the Critical Sizes for Shear Band Formation in Metallic Glasses from Molecular Dynamics Simulation. *Appl. Phys. Lett.* **2007**, *91* (23). https://doi.org/10.1063/1.2821832.

(21) Shi, Y. Size-Independent Shear Band Formation in Amorphous Nanowires Made from Simulated Casting. *Appl. Phys. Lett.* **2010**, *96* (12). https://doi.org/10.1063/1.3340908.

(22) Shi, Y.; Falk, M. L. Stress-Induced Structural Transformation and Shear Banding during Simulated Nanoindentation of a Metallic Glass. *Acta Mater.* **2007**, *55* (13), 4317–4324. https://doi.org/10.1016/j.actamat.2007.03.029.

(23) Xiao, Q.; Huang, L.; Shi, Y. Suppression of Shear Banding in Amorphous ZrCuAl Nanopillars by Irradiation. *J. Appl. Phys.* **2013**, *113* (8). https://doi.org/10.1063/1.4793562.

(24) Chen, I.-C.; Kelly, J. P.; Novitskaya, E.; Eliasson, V.; Hodge, A. M.; Graeve, O. A. Mechanical Properties of an Fe-Based SAM2x5-630 Metallic Glass Matrix Composite with Tungsten Particle Additions. *Adv. Eng. Mater.* **2018**, *20* (9), 1–10. https://doi.org/10.1002/adem.201800023.

(25) Farmer, J.; Choi, J.-S.; Saw, C.; Haslam, J.; Day, D.; Hailey, P.; Lian, T.; Rebak, R.; Perepezko, J.; Payer, J.; Branagan, D.; Beardsley, B.; D'amato, A.; Aprigliano, L. Iron-Based Amorphous Metals: High-Performance Corrosion-Resistant Material Development. *Metall. Mater. Trans. A* **2009**, *40* (6), 1289–1305. https://doi.org/10.1007/s11661-008-9779-8.

(26) Khanolkar, G. R.; Rauls, M. B.; Kelly, J. P.; Graeve, O. A.; Hodge, A. M.; Eliasson, V. Shock Wave Response of Iron-Based in Situ Metallic Glass Matrix Composites. *Sci. Rep.* **2016**, *6* (22568), 1–9. https://doi.org/10.1038/srep22568.

(27) Graeve, O. A.; Saterlie, M. S.; Kanakala, R.; Torre, S. D. de la; Farmer, J. C. The Kinetics of Devitrification of Amorphous Alloys: The Time–Temperature–Crystallinity Diagram Describing the Spark Plasma Sintering of Fe-Based Metallic Glasses. *Scr. Mater.* **2013**, *69* (2), 143–148. https://doi.org/0.1016/j.scriptamat.2013.02.019.

(28) Farmer, J. C.; Choi, J.-S.; Saw, C.-K.; Rebak, R. H.; Day, S. D.; Lian, T.; Hailey, P. D.; Payer, J. H.; Branagan, D. J.; Aprigliano, L. F. Corrosion Resistance of Amorphous $Fe_{49.7}Cr_{17.7}Mn_{1.9}Mo_{7.4}W_{1.6}B_{15.2}C_{3.8}Si_{2.4}$ Coating: A New Criticality Control Material. *Nucl. Technol.* **2008**, *161* (2), 169–189. https://doi.org/10.13182/NT08-A3921.

(29) Schroers, J. Processing of Bulk Metallic Glass. *Adv. Mater.* **2010**, *22* (14), 1566–1597. https://doi.org/10.1002/adma.200902776.

(30) Fecht, H. J. Thermodynamic Properties of Amorphous Solids -Glass Formation and Glass Transition- (Overview). *Mater. Trans.* **1995**, *36* (7), 777–793. https://doi.org/10.2320/matertrans1989.36.777.

(31) Herlach, D. M. Containerless Undercooling and Solidification of Pure Metals. *Annu. Rev. Mater. Sci.* **1991**, *21* (1), 23–44. https://doi.org/10.1146/annurev.ms.21.080191.000323.

(32) Busch, R.; Schroers, J.; Wang, W. H. Thermodynamics and Kinetics of Bulk Metallic Glass. *MRS Bull.* **2007**, *32* (8), 620–623. https://doi.org/10.1557/mrs2007.122.

(33) Schroers, J. On the Formability of Bulk Metallic Glass in Its Supercooled Liquid State. *Acta Mater.* **2008**, *56* (3), 471–478. https://doi.org/10.1016/j.actamat.2007.10.008.

(34) Yan, W.; Richard, I.; Kurtuldu, G.; James, N. D.; Schiavone, G.; Squair, J. W.; Nguyen-Dang, T.; Das Gupta, T.; Qu, Y.; Cao, J. D.; Ignatans, R.; Lacour, S. P.; Tileli, V.; Courtine, G.; Löffler, J. F.; Sorin, F. Structured Nanoscale Metallic Glass Fibres with Extreme Aspect Ratios. *Nat. Nanotechnol.* **2020**, *15* (10), 875–882. https://doi.org/10.1038/s41565-020-0747-9.

(35) Kündig, A. A.; Schweizer, T.; Schafler, E.; Löffler, J. F. Metallic Glass/Polymer Composites by Co-Processing at Similar Viscosities. *Scr. Mater.* **2007**, *56* (4), 289–292. https://doi.org/10.1016/j.scriptamat.2006.10.019.

(36) Painting Valley. Fiber Drawing Image 28 https://paintingvalley.com/download-image#fiber-drawing-28.png.

(37) Matweb. Schott AR-Glas Soda Lime Silicate Glass http://www.matweb.com/search/DataSheet.aspx?MatGUID=c72a11187fb34d8cadb600a0706aba69.

(38) Matweb. Schott Glass 8095 Lead Glass http://www.matweb.com/search/datasheet.aspx?matguid=2873442d080b4979a169d45e7a2dee55&ckck=1.

(39) Matweb. Corning Pyrex 7740 Borosilicate Glass Sheet http://www.matweb.com/search/DataSheet.aspx?MatGUID=5bb651ca58524e79a503011b2cd8083d.

(40) NASA. Concervation of Mass https://www.grc.nasa.gov/www/k-12/airplane/mass.html.

(41) Kostecki, R.; Ebendorff-Heidepriem, H.; Warren-Smith, S. C.; Monro, T. M. Predicting the Drawing Conditions for Microstructured Optical Fiber Fabrication. *Opt. Mater. Express* **2014**, *4* (1), 29. https://doi.org/10.1364/ome.4.000029.

(42) Yazdani, A.; Höhne, G. W. H.; Misture, S. T.; Graeve, O. A. A Method to Quantify Crystallinity in Amorphous Metal Alloys: A Differential Scanning Calorimetry Study. *PLoS One* **2020**, *15* (6), 1–31. https://doi.org/10.1371/journal.pone.0234774.

(43) Kelly, J. P.; Fuller, S. M.; Seo, K.; Novitskaya, E.; Eliasson, V.; Hodge, A. M.; Graeve, O. A. Designing in Situ and Ex Situ Bulk Metallic Glass Composites via Spark Plasma Sintering in the Super Cooled Liquid State. *Mater. Des.* **2016**, *93*, 26–38. https://doi.org/10.1016/j.matdes.2015.12.130.

(44) Farmer, J. C.; Haslam, J. J.; Day, S. D.; Lian, T.; Saw, C. K.; Hailey, P. D.; Choi, J.-S.; Rebak, R. B.; Yang, N.; Payer, J. H.; Perepezko, J. H.; Hildal, K.; Lavernia, E. J.; Ajdelsztajn, L.; Branagan, D. J.; Buffa, E. J.; Aprigliano, L. F. Corrosion Resistance of Thermally Sprayed High-Boron Iron-Based Amorphous-Metal Coatings: Fe 49.7 Cr 17.7 Mn 1.9 Mo 7.4 W 1.6 B 15.2 C 3.8 Si 2.4. *J. Mater. Res.* **2007**, *22* (8), 2297–2311. https://doi.org/10.1557/jmr.2007.0291.